UNIVERSIDAD DE CHILE
FACULTAD DE CIENCIAS FÍSICAS Y MATEMÁTICAS
DEPARTAMENTO DE INGENIERÍA MECÁNICA

EVALUATION OF AN ANALYTICAL MODEL OF FRICTION STIR WELDING

MEMORIA PARA OPTAR AL TÍTULO DE INGENIERA CIVIL MECÁNICA

MAGDALENA ESTELA URRUTIA UNDA

PROFESOR GUÍA:
Patricio Mendez Pinto

MIEMBROS DE LA COMISIÓN:
Rubén Fernandez Urrutia
Williams Calderón Muñoz

Este trabajo ha sido parcialmente financiado por el Gobierno Canadiense a través de la beca "Emerging Leaders in the Americas Program"

SANTIAGO DE CHILE
2022

RESUMEN DE LA MEMORIA PARA OPTAR
AL TÍTULO DE INGENIERA CIVIL
MECÁNICA
POR: MAGDALENA ESTELA URRUTIA UNDA
FECHA: 2022
PROF. GUÍA: PATRICIO MENDEZ PINTO

Evaluación de un modelo analítico de soldadura por fricción y agitación

La soldadura por fricción y agitación (FSW) es una técnica de unión avanzada en la cual, la soldadura de dos piezas se produce en estado sólido, sin necesidad de fundir el metal. Este proceso de soldadura presenta actualmente una serie de aplicaciones relacionadas a la industria aeroespacial, tales como el fuselaje de aviones, naves y diferentes componentes de cohetes. Mediante este trabajo se busca acercar los conceptos teóricos de FSW para una mejor representación del proceso de soldadura práctico, ya que su desarrollo previo se ha llevado a cabo principalmente en base a prueba y error. Lo anterior se logra integrando diferentes áreas de la ingeniería, como transferencia de calor e ingeniería de materiales. El principal objetivo de este trabajo se compone de tres partes. En primer lugar se tiene que validar el modelo fenomenológico planteado por el Dr. Mendez, para un conjunto de metales. Por otro lado, se debe extender el modelo mediante la adición de una cuarta simplificación representativa del proceso. Por último se deben afinar los valores característicos desarrollados, mediante la incorporación de factores de corrección empíricos. Para evaluar la precisión del modelo, las estimaciones realizadas se comparan con los resultados numéricos y de medición recopilados en la base de datos, para cada una de las simplificaciones del proceso. Como resultado general se obtiene que el modelo logra capturar las tendencias y ordenes de magnitud adecuados de los valores reportados de temperatura máxima y torque. Si bien las estimaciones realizadas por el modelo tienen un nivel de dependencia en algunas de las simplificaciones, la aplicación de las respectivas funciones de corrección permite contrarrestar este comportamiento y lograr estimaciones más exactas.

RESUMEN DE LA MEMORIA PARA OPTAR
AL TÍTULO DE INGENIERA CIVIL
MECÁNICA
POR: MAGDALENA ESTELA URRUTIA UNDA
FECHA: 2022
PROF. GUÍA: PATRICIO MENDEZ PINTO

Evaluation of an analytical model of friction stir welding

Friction stir welding (FSW) is an advanced joining technique in which two pieces are welded in a solid state, without the need to melt the metal. This welding process currently presents a variety of applications related to the aerospace industry, such as the fuselage of airplanes, ships and different rocket components. Through this work, it is sought to approach the theoretical concepts of FSW for a better representation of the practical welding process, since its previous development has been carried out mainly on a trial-error basis. The above is achieved by integrating different areas of engineering, such as heat transfer and materials engineering. The main objective of this work consists of three parts. In the first place, the phenomenological model proposed by Dr. Mendez must be validated for a set of metals. On the other hand, the model must be extended by adding a fourth simplification representative of the process. Finally, the characteristic values developed must be tuned by incorporating empirical correction factors. To evaluate the accuracy of the model, the estimations are compared to the measurement and numerical results collected in the database, for each of the simplifications of the process. As a general result, it is obtained that the model manages to capture the proper trends and orders of magnitude of the reported values of maximum temperature and torque. Although the estimations performed by the model have a level of dependence on some of the simplifications, the application of the respective correction functions allows to counteract this behavior and achieve more exact estimations.

To my mother,
who has always taken care of me from wherever she is.

Acknoledgments

Among all those who have contributed to my academic formation and to this work, I would like to thank my father, Osvaldo Urrutia, who is the person I admire the most in this world. Thank you for motivating me to pursue my dreams and being a essential support even in the most difficult times.

I would like to thank my aunt María Unda. Thank you for receiving me in your life as a 3 year old girl, for raising me and teaching me what discipline and hard work is. I thank my godmother and aunt Mirtha Unda, for giving me her love and chocolates every time I was feeling down. I would also like to thank my aunt Magaly Unda, for always listening and being a great support for me, especially with our video calls during my months in Canada. Lastly, thank to all the members of my family, for believing in me and being a source of inspiration and love during all these years.

I thank all the teachers that have contributed to my formation and saw potential in me, during my school and university years. You are responsible for my passion for learning and educating myself. Above all, I would like to thank Dr. Patricio Mendez, for giving me the opportunity to participate in his research, being a constant source of motivation and introducing me to the welding field. I feel truly fortunate to have developed my thesis on such a fascinating topic. I would also like to thank Dr. Ruben Fernandez for his willingness to answer my questions during the writing period of this thesis.

I would like to thank my friends of my first years of university, especially Vicente Neira, Salomé Huerta, Rodrigo Arenas and Carla Garrido. Thanks for all the joy you have brought to me and for making my university experience one of the best stages in my life. I thank my friends from mechanical engineering, thank you for living with me all these years of effort and filling them with laughter and good energy. I thank the friends I made in Canada, this little group that made my internship an unforgettable experience. I especially would like to thank my friend Sofia Salazar, for teaching me everything to survive in a foreign country and being a constant support while doing my thesis. I would also like to thank my friends from school, for continuing to give me their friendship during all these years. Lastly, thank to the people I met in the memoirists room, for all the conversations and good moments shared these last months.

Table of Content

List of Tables

List of Figures

Chapter 1

Introduction

Welding plays an essential role in the assembly of components, furthermore, it can be said that nowadays there is almost no industry that can dispense with this joining technique. Whether in the automotive, petrochemical, medical, or even jewelry industries, a wide variety of processes that require this form of union can be found. It is paradoxical, however, that despite being an essential tool in multiple industries, its development has been based on trial and error, instead of knowing and understanding the physical phenomena that occur behind this process. With the above, the motivation for this work is to approach the theoretical concepts of welding for a better representation of the practical welding process, thereby integrating different areas of engineering, such as heat transfer and materials engineering.

Currently, there is a wide variety of welding methods, some of them are diffusion welding, gas tungsten arc welding (GTAW), inert gas welding (MIG), friction stir welding (FSW), laser beam welding (LBW), plasma arc welding (PAW), among others. Depending on the application sought, it is that a certain method is chosen over another. In the case of friction stir welding, it is used to weld metals in which it is essential not to melt the base material, as is the case of aluminum, which, when welded by conventional methods, tends to burn easily, while with friction and stir welding, the union is achieved while maintaining the mechanical properties of the material.

The welding methods that melt the base material affect its mechanical properties, since, when the metal reaches its melting temperature, the grain will form again within the structure of the material, and depending on the cooling time, secondary phases arise, such as martensite, which implies that the welded area will have a different internal structure than the base material, this at the same time can generate surface defects, such as fissures. This problem does not occur in the case of friction stir welding, since the principle behind this method consists of welding the material through plastic deformation by friction. With the above, the friction produced between the tool and the pieces to be welded causes the latter to heat below their melting point, thus presenting a fluidized behavior, which allows the joining

of the pieces.

Friction stir welding presents a series of advantages, among which are that there is no presence of toxic fumes or spatter of molten material. In addition, dissimilar materials can be welded, since solidification does not occur, furthermore, there is no weld pool, therefore the process can be done in all positions, and it has a low environmental impact.

The most relevant applications of friction stir welding are found in the aerospace industry, automotive, construction, or similar. For example, in the aerospace industry, the fabrication of structures in the fuselage of rockets is performed, while, in the automotive industry, FSW is used for the manufacture of components for heavy vehicles such as steering shafts, transmission gears, among others. On the other hand, in the construction industry, this welding technique is used for joining machinery pieces such as cylinders and hydraulic rods, or rotating parts and control rollers.

1.1. Objectives

The general objective of this work is to validate the phenomenological model proposed by Mendez, Tello, and Lienert [1] modified by Salazar [2], for an expanded set of materials, as well as to extend it by integrating an additional simplification representative of the process and to tune the developed characteristic values, by incorporating empirical correction factors. To achieve the above, the following specific objectives must be accomplished:

- Expand the original FSW database by adding a series of new experiments.
- Incorporate the fourth assumption corresponding to the relation between the preheat temperature due to the shoulder friction and the maximum temperature at the pin/shear layer interface.
- Analyze the temperature and torque with the four simplifications that the mentioned model contemplates.
- Tune the estimations of temperature and torque to increase their accuracy by determining correction functions.
- Analyze the measurements to the estimations with and without the correction function improvement.

1.2. Motivation

Although the aerospace industry is a newly developing field, it has become an important part of the technological advances of the XX and XXI centuries. Within this area, the materials with which the different space vehicles are manufactured are of vital importance, as

they must be light but resistant. This is the case of aluminum, which by having a higher thermal conductivity and a low melting point, has a smaller workability window than other metals, this can cause the material to burn before it melts properly.

Friction stir welding turns out to be the optimal method for welding metals such as aluminum, since, as the metal does not melt, it is prevented from suffering burns and in turn has the benefit of maintaining the mechanical properties of the material. This is advantageous since problems such as porosity, the presence of coarse grains, and distortions, among others, are avoided.

With all the above, it is vitally important to perform studies and research in friction stir welding and thereby be able to develop equations that can be used in a simple way in the industry. Thus, the motivation of this work focuses on approaching the theoretical concepts of welding to describe the FSW process, integrating with this, different areas such as heat transfer and materials engineering.

1.3. Scope of work

The process is considered in a general way, studying the plastic deformation and heat transfer, taking as a basis the four simplifications that govern the welding process and leaving out phenomena such as recrystallization, precipitation, intermetallic formation, etc.

The main resource of this work is a database that has multiple experiments obtained from the literature, which do not take into account defects such as the existence of pores or environmental conditions. Additionally, it is sought to expand this database with new experiments on already present materials and new materials through bibliographic research.

On the other hand, the mathematical model used in this work only considers a cylindrical threaded type of pin. Similarly, the heat losses through the working took are left out of scope.

Chapter 2

Background

2.1. Friction stir welding

Friction stir welding is a solid-state welding process in which a non-consumable rotating tool has the task of welding two pieces through mechanical deformation by friction.

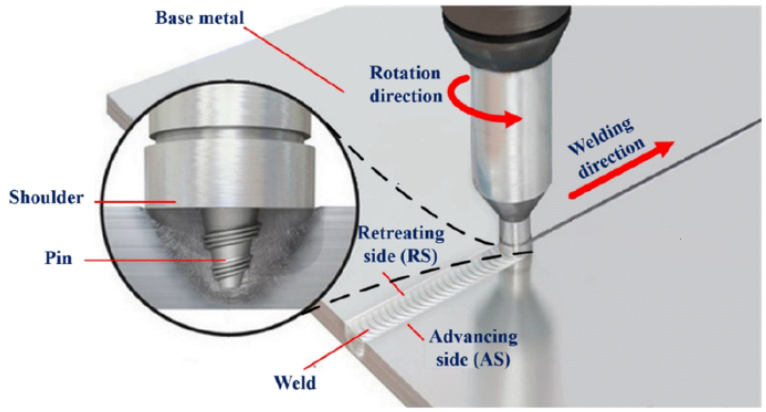

Figure 2.1: FSW process schematic and typical working tool.

The rotating tool is composed of a shoulder and a pin that penetrates the joint and rotates as it moves along the joint of the two plates. The agitation generated by the pin and the pressure exercised by the shoulder on the plates allows them to deform and mix, consolidating their union. On the other hand, due to its larger diameter, the shoulder fulfills a preheating function. This happens because this part of the tool rotates and hence produces friction as well, which confers heat to the plates before the pin, and allows the latter to advance with ease.

Other components present in this welding technique are the advancing side, associated with the zone of rotation of the pin in the same direction as the fluidized material, and the retreating side, which is associated with the zone of rotation of the pin in the opposite direction [3]. Additionally, the zone in which the weld is generated is called the deformation zone.

The main advantages of this process are the absence of solidification defects such as the formation of pores produced by interdendritic contractions. This mainly happens since the fusion of the material does not occur, which in turn maintains properties such as resistance and plasticity, without the need to undergo heat treatments. It should also be noted that this is an autogenous welding type, which means that no filler material is needed. Finally, friction stir welding does not make use of shielding gases.

A restriction of this type of welding is that the pin requires resisting the friction and heat of the process, so it is recommended to apply the process to low melting temperature materials. Another limitation is that this process must be automated since it involves high forces and velocities. On the other hand, both at the beginning and at the end of the process defects usually arise. Despite the above, it is worth mentioning that the plates to be welded can be joined regardless of their position, since there is no fusion of the material there is no risk of run-off of the molten material.

2.2. Models and methods of FSW

There are multiple studies that seek to understand the process of friction stir welding, and with it to make known the optimal parameters to implement in its application. Within these studies different models and methods have been used to characterize FSW welding, there are numerical and analytical models that have managed to develop temperature distribution analysis in the welding zone, heat flows, welding velocities, among others.

Between the different analyses performed is the steady state heat transfer analysis, using the finite element method, which allows modeling the heat transfer of the normal and cold FSW welding, both at the union of two aluminum alloy plates and in the welding tool [4]. On the other hand, coupled numerical models are employed, through the use of CFD simulation, for which there is developed a model that includes thermal analysis, coupled flow analysis, and heat generation by viscose dissipation, among others. This predicts the welding temperature and welding power [5].

Another tool used is scaling analysis, employed in a study that consists of nondimensionalize the variables of the equations that govern the FSW welding process. The study implements FEM simulation to provide time-temperature histories for a series of welds made of aluminum alloy [6], from which relations are drawn such as that the heating and cooling rates associated with a given weld are determined by the welding velocity.

Similarly, the model for friction stir welding developed by Méndez, Tello and Lienert [1] uses scale analysis to treat heat transfer and plastic deformation in welding, which leads to the development of expressions that allow obtaining the torque of the pin, the thickness of

the shear layer, the maximum temperature, and the heat generation.

Another aspect of interest in FSW turns out to be the contact condition between the material and the working tool, for which two cases are suggested. In the first place, there is the slip condition, in which the material only undergoes elastic deformation, since the contact shear stress is smaller than the material yield shear stress. In contrast, there is the sticking condition, in which the contact shear stress exceeds the yield shear stress of the material [7], therefore part of the material is going to stick to the rotative tool. On the other hand, it is currently debated whether the heat is generated is the product of coulombic mechanisms at the tool/base plate interface, implying the sliding condition, or by plastic deformation in the shear layer in case there is sticking condition, or even a combination of both.

A study of the material flow using the tracer technique [8] concluded that the sticking condition on the tool/workpiece interface is predominant. Ulysse [9], Seidel and Reynolds et al. [10] along with others [5, 11], presented models that only consider the sticking condition. Additionally, Xu et al. [12], suggested a model of the interface between pin and the base plate in which it is stated that the contact zone between the pin and the surrounding material is mainly a slipping interface. Chao et al. [4] and McClure et al. [13] proposed as well models that contemplate sliding friction.

Finally, it has been debated over the years whether the heat of the process is generated by the pin or the shoulder. Mc Clure et al. [13] and Chao et al. [4] propose that the shoulder is primarily responsible for heat generation, while others [14, 15, 16] suggest that heat is generated by a combination of both. Schmidt et al. [7] proposed heat transfer models by conduction and concluded that most of the heat generation is produced by the shoulder. Similarly, Chao et al. [4] worked on a heat transfer model by convection and concluded that 5 % of the heat generated dissipated in the tool.

2.3. List of symbols

Symbols	Description
Pe	Peclet number
V	Travel speed of the pin [m/s]
ω	Rotational speed of the pin [s^{-1}]
a	Pin radius [m]
b	Shoulder radius [m]
t	Thickness of the plate [m]
δ	Thickness of the shear layer[m]
τ_c	Shear stress within the shear layer [Pa]
k_o	Thermal conductivity of the plate associated to the temperature To[W/mK]
K_o	Modified Bessel function of the second kind and order 0
T_o	Temperature of the shear layer/base plate interface [K]
T_p	Preheat temperature due to the shoulder friction[K]
ΔT_s	Temperature difference T_s - T_o [K].
T_s	Maximum temperature at the pin/shear layer interface [K]
T_m	Melting temperature of the base plate (solidus temperature) [K]
T_∞	Initial temperature of the base plate [K]
α_δ	Thermal diffusivity of the plates at T_o [m2/s]
η	Total efficiency of the process, which accounts for heat losses in the form of energy stored as dislocations in the shear layer and heat lost to the tool.
η_s	Efficiency that accounts for the fraction of the mechanical energy converted into heat, excluding the small amount of mechanical energy that is accumulated as potential energy in the form of dislocations.
ΔT_o	Temperature difference T_o - T_∞ [K].
R	Gas constant [J/mol K]
A	Constant of the Zener-Hollomom law [s^{-1}]
Q	Constant of the Zener-Hollomom law. Activation energy [J/mol]
n	Constant of the Zener-Hollomom law
τ_R	Reference shear stress [Pa]
σ_R	Reference normal stress [Pa]
τ	Shear stress experienced by an element of volume at coordinate x [Pa]
$\widehat{q_c}$	Estimation of the volumetric heat generation within the shear layer [W/m^3]
$\widehat{\tau_c}$	Estimation of the shear stress within the shear layer [Pa]
$\widehat{\delta}$	Estimation of the shear layer thickness [m]
$\widehat{M}$	Estimation of torque of the pin [Nm]
$\widehat{T_s}$	Estimation of the maximum temperature [K]
ξ	Variable that considers the heat loss through the plate.

2.4. Simplifications of the model

The coupled model considers the interaction between plastic deformation and heat transfer, and is restricted to the shear layer around a threadless cylindrical pin. Figure (2.2) illustrates the different variables that constitute the model.

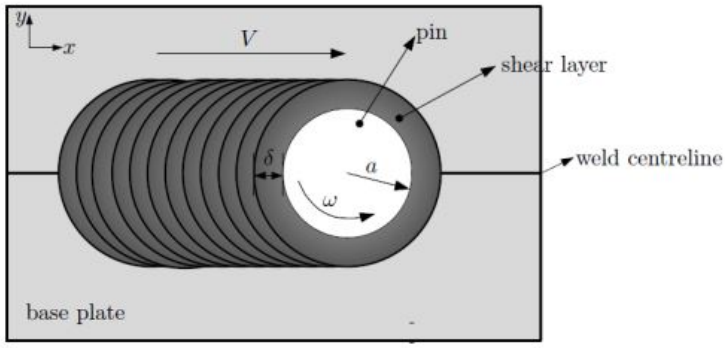

Figure 2.2: Schematic of FSW including the shear layer.

In first place there are the pin and shoulder diameter 'a' and 'b' respectively; the shear layer thickness 'δ' corresponding to the friction stir welded region; the traveling and rotational speeds 'V' and 'ω' respectively.

The first simplification states that the traveling speed of the heat source can be approximated to a steady state, slow moving source, with which the form of the isotherms can be considered as a circular shape. This is based on Rosenthal's solution [17] and allows to estimate the heat transfer to the base plate as a function of the Peclet number:

$$Pe = \frac{Va}{2\alpha} << 1 \tag{2.1}$$

The second simplification compares the deformation of the shear layer to the viscous layer of a body moving through a fluid, since the viscous boundary layer can be represented as the region where the inertial and viscous forces are balanced. Likewise, the shear layer can be assumed as the area in which the heat generation and heat conduction are in equilibrium, and since the heat generated is lower than the melting temperature, it is stated that the shear layer is considerably thinner than the pin diameter:

$$\delta << a \tag{2.2}$$

The third assumption states that the travel velocity is significantly lower than the rotational velocity, this allows to assume radial symmetry in the shear layer, since the amount of material that enters the deformation ($\approx \mathrm{V} \cdot a$) is much smaller than that which is deformed by the revolutions ($\approx \cdot\, \omega \cdot a \cdot \delta$), which can be expressed as the following:

$$\rho \cdot V \cdot a << \rho \cdot \omega \cdot a \cdot \delta \Leftrightarrow V << \omega \cdot \delta \tag{2.3}$$

A fourth assumption is incorporated to the model. This one proposes that the heat promoted by the shoulder to the maximum temperature near the pin is negligible compared to the heat concentrated from the deformation around the pin:

$$T_p - T_\infty << T_s - T_\infty \tag{2.4}$$

Chapter 3

Materials and methods

3.1. Methodology

This work is based on the coupled model proposed by Mendez, Tello and Lienert in the publication "Scaling of coupled heat transfer and plastic deformation around the pin in friction stir welding"[1], which was modified by Salazar [2] to include the mathematical variable of heat loss. With the above, the main contribution of this thesis consists of the realization of three major tasks which are specified as follows:

1. Validating the accuracy of the coupled model, for an expanded set of materials.

   To accomplish this, the mathematical model from the Mendez, Tello and Lienert publication must be studied and inspected, and then, with a better understanding of parameters required to apply the equations, the following is to examine relevant literature (theses, papers, articles) that contain friction stir welding experiments or simulations for both new and existent materials to the database. From the above, a series of parameters (such as velocities and tool dimensions) can be extracted, as well as the results of the measurements made (maximum temperature and torque). On the other hand, by adding information about new materials, there will be required to obtain their Zenner-Hollomon constants. The latter is achieved by searching for the particular values for each material in books or articles. In the case of materials for which the constants are not found, values of materials with similar properties will be used. Another requirement is to find the thermophysical properties (heat capacity, thermal conductivity, density) of the new materials, which can be obtained from the *JmatPro* software. However, the properties are delivered in moles, whereby the molar masses of all the new materials will have to be calculated to convert the values to SI units. Finally, with all the parameters, constants and properties obtained, the values of $\widehat{\delta}$, $\widehat{\tau_c}$, $\widehat{T_s}$ and $\widehat{M}$ can be calculated for each experiment.

2. Applying the fourth criterion related to the preheat temperature due to the shoulder friction and the maximum temperature at the pin/shear layer interface.

   Among the parameters obtained from the literature inspection specified in the previous

step, the values of V, ω, a and α can be found. On the other hand, the results of $\widehat{\delta}$ and $\widehat{T_s}$, are already calculated for each experiment. With all the above the values of the four simplifications that represent the model (listed below) can be obtained.

- Pe«1
- $\widehat{\delta}/a$«1
- $V/\omega\delta$«1
- $T_P - T_\infty/\widehat{T_s} - T_\infty$«1

The following step is to elaborate the graphs that compare the ratios of máximum temperature and torque ($(T_s - T_\infty)/(\widehat{T_s} - T_\infty)$ and $M/\widehat{M}$ respectively), to the four simplifications exposed previously, for the experiments belonging to the expanded database.

3. Determining correction factors to tune the results of the estimations.

   With all the graphs mentioned above, it must be verified whether the ratios remain constant through the 'X' axis. If the ratios begin to deviate from the asymptotic regime, a correction function must be formulated to counteract the influence of the simplification on the estimation. The minimum least squares model is applied between the calculated ratios and a correction function, which depends on a series of coefficients that are the ones that must be optimized. Finally the estimations with and without the tuning from the correction functions are compared against $(T_s - T_\infty)$ and M respectively, though graphs that allow to establish which option is more accurate.

3.2. Resources

The resources used for this work are the following:

- Matlab: Software used to build the graphs.
- Excel: Software that contains the database and its associated calculations.
- Bibliographic material: Publications with experimental information of FSW.
- JmatPro: Software used to obtain the thermophysical properties of the new materials

3.3. Database

The database consists of publications with the necessary information to calculate the estimations of maximum temperature and torque, in order to compare them to the experimentally measured or computer simulated data,

The database originally consisted of the following materials:

- Al2024
- Al2195
- Al5083
- Al6061
- Al7050
- Al7075
- AISI 1018
- AISI 304
- Ti-6Al-4V

Meanwhile the new materials added to the database are the following:

- AA1080
- AA2198
- AA2199
- AA2219
- AA2524
- AA5059
- AA6082
- AA7010
- AA7020
- AA7136
- SSA038
- IF Steel
- AISI 1012
- AISI 1035
- AZ31

Below is exposed how the different measurements were taken in the literature to clarify the origin of the database information.

- Temperature: It is possible to measure the temperature, by using a k-type thermocouple coupled to the plate in different heights of its width and length, thus, the temperature profile and its evolution over time can be obtained. In other cases, the thermocouple is placed inside the rotative tool, for this purpose the smallest off-the-shelf K-type thermocouple is placed, so that the temperature response time decreases (sheath diameter 0.25 mm, part no. TJ36-CAXL-010U; Omega Corp.), in this case, there is also obtained the variation of the temperature (with a proportional variation in contrast with the temperature measured in the plate). Finally, the temperature can be measured as well by infrared cameras (Mikron M7815 Infrared Thermal Imaging Camera) or thermoelectric methods.

- Force and Torque: Force and torque measurements are made through the use of a dynamometer, load cells (SEWHA, 2000kg capacity, R.O:2.0008mV/V or LowStir™ device) and strain gauge. Other less frequent methods consist in energy measurements from which torque and forces can be obtained.

Chapter 4

Development of the coupled model

4.1. Scaling of the coupled thermal and mechanical problem

In isothermal models of the shear layer, there is the implicit assumption that the characteristic length scales for heat transfer and plastic flow are of a different order of magnitude, being the length scale for heat transfer much larger than for plastic flow.

The model proposed by Dr. Mendez establishes that heat transfer and plastic flow are coupled in the shear layer, meaning that both variations of temperature and velocities happen with the same length scale: the thickness of the shear layer δ. The above means that the heat generation and the deformation occur simultaneously in the shear layer.

To analyze the problem of interest, Dantzig and Tucker [18], Krantz [19] and Mendez [20] proposed scaling analysis. This method consists of replacing the ordinary differential equations that describe the problem with a system of four algebraic equations with four unknowns. Each of which has a characteristic value of a function or differential expression. In the following sections, it is explained that the algebraic equations were obtained by analyzing heat transfer and plastic flow in the shear layer, heat transfer in the base plate, kinematic constraints to plastic flow, and the constitutive behavior of the base plate material.

4.1.1. Heat conduction in the shear layer

In Figure (4.1 (a)) it can be seen that the temperature decreases monotonically, starting from the maximum temperature value at the tool/shear layer interface (T_s at x = 0) to T_o at the shear layer/base plate interface (x = δ). With the above, the base plate can be divided in two regions: the shear layer, where most deformation occurs, and the rest of the base plate, where no significant shearing occurs. It can be said that the temperature transition between the mentioned regions is gradual and can be represented by the characteristic value of T_o. Additionally, it is worth mentioning that the secondary effect of heat losses from the base

plate into the tool is neglected.

In Figure (4.1 (b)) it can be seen that the tangential velocity profile in the shear layer decreases gradually, starting from a maximum value at the tool/shear layer interface ($\omega \cdot a$ at x = 0) to zero in the region furthest from the shear layer. The velocity transition between the mentioned regions is gradual, but the model states ideally that the tangential velocity is zero in the shear layer/base plate interface (x = δ).

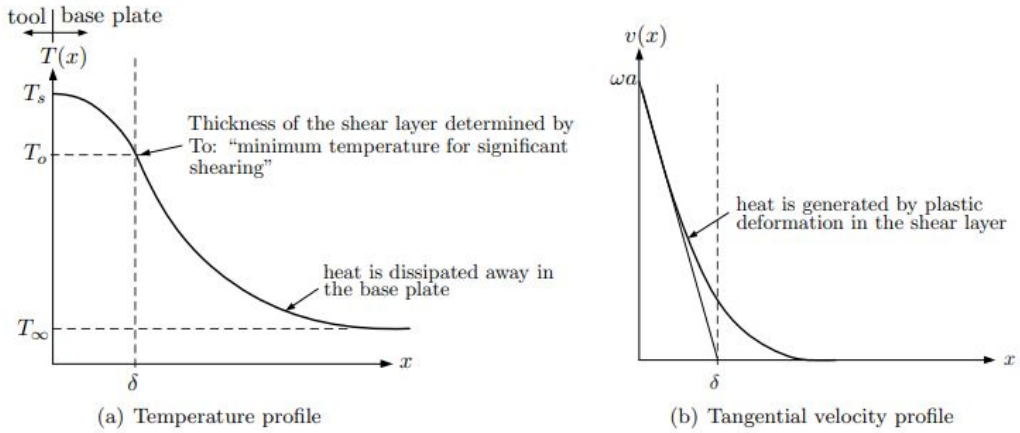

Figure 4.1: Coupling of heat transfer and plastic flow with both of them having the thickness of the shear layer as characteristic length .

The heat transfer and the plastic deformation around the pin can be taken as a one-dimensional problem, based on the simplifications made in Section (2.4)). The one-dimensional problem is illustrated in Figure (4.2), where the x coordinate is found perpendicular to the pin/base plate interface and originates at that interface.

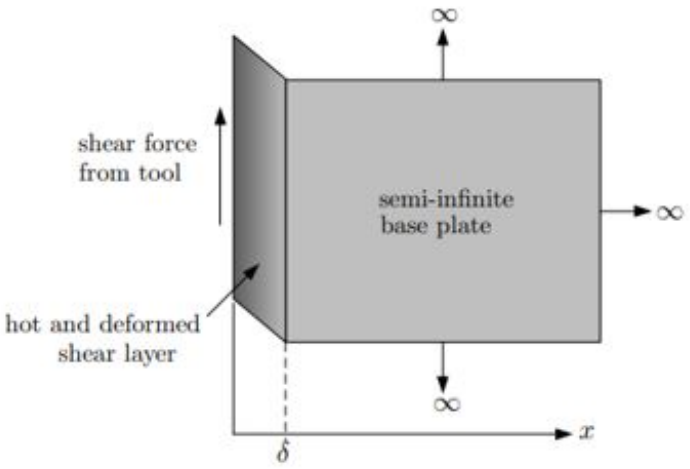

Figure 4.2: Illustration of the one-dimensional problem, where the pin/shear layer interface is located at x = 0.

The expression of conservation of energy for the steady-state, low Peclet and one-dimensional problem exposed in the previous section is given by Equation (4.1).

$$\frac{\mathrm{d}^2 T}{\mathrm{d}x^2} + \frac{q(x)}{k} = 0 \tag{4.1}$$

where $T(x)$ is the temperature profile in the shear layer, $q(x)$ is the volumetric heat generation due to plastic deformation, and $k(T)$ is the thermal conductivity of the base plate. The equation assumes a balance between the heat conduction, represented by the first term, and the volumetric heat generation, represented by the second term. The boundary conditions are the following.

$$\left.\frac{\mathrm{dT}}{\mathrm{d}x}\right|_{x=0} \approx 0 \tag{4.2}$$

$$T|_{x=\delta} = T_o \tag{4.3}$$

The Equation (4.2) states that the heat lost to the tool does not significantly affect the temperature profile. This approximation is good for aluminum alloys, but in the case of alloys with lower heat conductivity, such as titanium, the condition might need to be reviewed, since in these cases the heat losses into the tool are more relevant. Equation (4.3) contains the term T_o, which represents the temperature below which there is no significant shear rate.

The two terms of Equation (4.1) can be normalized by an estimation of their maximum values given by the following.

$$x = \widehat{\delta} x* \tag{4.4}$$

$$\frac{\mathrm{d}^2\mathrm{T}}{\mathrm{d}x^2} = 2\frac{\Delta\widehat{T_s}}{\widehat{\delta}^2}\left(\frac{\mathrm{d}^2\mathrm{T}}{\mathrm{d}x^2}\right)^* \tag{4.5}$$

$$q(x) = \widehat{q_c} q^*(x^*) \tag{4.6}$$

$$K(T) = k_0 k^*(T^*) \tag{4.7}$$

Where the values with an asterisk are normalized functions. The expressions from above can be replaced on Equation (4.1), to obtain the normalized equation of conservation of energy.

$$2\frac{\Delta\widehat{T_s}}{\widehat{\delta}^2}\left(\frac{\mathrm{d}^2\mathrm{T}}{\mathrm{d}x^2}\right)^* + \frac{\widehat{q_c}}{k_o}\left(\frac{q}{k}\right)^* = 0 \tag{4.8}$$

The hat notation refers to estimations of the characteristic values, which are not exactly equal to the actual characteristic values since they are the outcome of simplified algebraic equations. The normalized functions have an approximated maximum absolute value of 1 at x=0 since they have been normalized by an estimation of their maximum values. The factor of 2 that accompanies the normalization of the second derivative represents the parabolic-like evolution of temperature within the shear layer.

The normalized functions can be replaced by +1 or -1, depending on the sign of the normalized function [18–20] . Thus, Equation (4.8) becomes the following algebraic expression based on the estimated values of their characteristic values, which are noted by the hat symbol as: $\Delta\widehat{T_s}$, $\widehat{\delta}$ and $\widehat{q_c}$.

$$-2\frac{\Delta\widehat{T_s}}{\widehat{\delta}^2} + \frac{\widehat{q_c}}{k_o} = 0 \tag{4.9}$$

4.1.2. Heat generation in the shear layer

Referring to the debate between the sticking and sliding boundary conditions at the tool/base plate interface, it is stated that only the sticking boundary condition occurs between the pin and the shear layer, leaving out the contribution of sliding friction. Under this hypothesis, the heat generated around the pin is produced solely by plastic deformation. Thus, the volumetric heat generated by the plastic deformation can be calculated as:

$$q(x) = \eta_s \tau(x)\dot{\gamma}(x) \tag{4.10}$$

Where $\tau(x)$ is the shear stress experienced by an element of volume at coordinate x, $\dot{\gamma}$ is the corresponding shear rate, η_s is the efficiency that accounts for the fraction of the mechanical energy converted into heat. The latter does not consider the small amount of mechanical energy that is stored as potential energy in the form of dislocations.

Taking into account that the shear stress varies little within the shear layer, as exposed in Equation (2.2), the shear layer is thin, and the shear stress varies inversely to the between the pin and shear layer radius, thus the variation is small and constant. Additionally, considering that the shear rate and tangential velocity gradient are essentially the same magnitude ($\dot{\gamma} = -dv/dx$), Equation (4.10) can be rewritten as the following:

$$q(x) = -\eta_s \tau \frac{dv}{dx} \tag{4.11}$$

$$v|_{x=0} = \omega a \tag{4.12}$$

Where Equation (4.12) represents its boundary condition, considering the tangential velocity profile exposed in Figure (4.1). The terms of Equation (4.11) are normalized by estimating their maximum values, as given in the next equations:

$$\frac{dv}{dx} = \frac{3}{2}\frac{\omega a}{\widehat{\delta}}\left(\frac{dv}{dx}\right)^* \tag{4.13}$$

$$\tau = \widehat{\tau}_c \tau^* \tag{4.14}$$

Replacing these terms into Equation (4.11), the normalized form of the volumetric heat

generation is the following:

$$\widehat{q_c}q^* = -\frac{3}{2}\eta_s\widehat{\tau_c}\frac{\omega a}{\widehat{\delta}}\left(\frac{dv}{dx}\right)^* \tag{4.15}$$

The factor of 3/2 observed in the equation relates to the evolution of velocity within the shear layer as presented in Figure (4.1). Finally, the normalized functions can be replaced by +1 or -1 and Equation (4.15) becomes the following expression:

$$\widehat{q_c} = \frac{3}{2}\eta_s\widehat{\tau_c}\frac{\omega a}{\widehat{\delta}} \tag{4.16}$$

The latter equation presents a new unknown characteristic value: $\widehat{\tau_c}$, thereby, the system has two Equations ((4.9) and (4.15)) and four unknowns ($\Delta\widehat{T_s}$, $\widehat{\delta}$, $\widehat{q_c}$ and $\widehat{\tau_c}$). To solve the system, two additional equations are required.

4.1.3. Constitutive equation in the shear layer

To compose the constitutive equation in the shear layer there must be assumed that no phase transformation occurs, such as remelting in the base plate. It is assumed that the material follows a Zener-Hollomon behavior. This constitutive model describes the combined effects of temperature and strain rate. Moreover, it has an intuitive interpretation based on activation energy and strain rate hardening which provides a good fitting for the existing high temperature and strain rate measurements. The Zener-Hollomon constitutive behavior is given by the following expression:

$$\dot{\gamma} = A\left(\frac{\tau}{\tau_R}\right)^n exp\left(-\frac{Q}{RT}\right) \tag{4.17}$$

Where 'A', 'Q', and 'n' are the parameters of the constitutive model, R is the gas constant, and τ_R is an arbitrary reference stress which gives consistent units to 'A'. Accounting that $T = T(x)$ and that $\dot{\gamma} = -dv/dx$, the Equation (4.17) can be normalized as the following:

$$-\frac{3}{2}\frac{wa}{\widehat{\delta}}\left(\frac{dv}{dx}\right)^* = A\left(\frac{\widehat{\tau_c}\tau^*}{\tau_R}\right)^n exp\left(-\frac{Q}{RT_s}\right) f^*(x^*) \tag{4.18}$$

$$v|_{x=0} = wa \tag{4.19}$$

Where Equation (4.19) is considered the boundary condition and $f^*(x^*)$ is given by:

$$f^*(x^*) = exp\left(-\frac{Q}{R}\left(\frac{1}{T(\widehat{\delta}x^*)} - \frac{1}{T_s}\right)\right) \tag{4.20}$$

Replacing the normalized functions by +1 or -1, Equation (4.18) turns into:

$$\frac{3}{2}\frac{\omega a}{\widehat{\delta}} = A\left(\frac{\widehat{\tau_c}}{\tau_R}\right)^n exp\left(-\frac{Q}{R\widehat{T_s}}\right) \tag{4.21}$$

To obtain a power law expression, another simplification can be made. In Figure (4.3) it is exposed that the exponential term of the constitutive equation can be divided into two asymptotic regimes. In the first place, there is the high-temperature regime, within the shear layer, near the pin and where the shear rate is high. In the second place, there is the low-temperature regime, which is outside the shear layer. The characteristic temperature T_o represents the limit between these two regimes. Close to the incipient melting temperature, the Arrhenius expression can be linearized as:

$$exp\left(-\frac{Q}{R\widehat{T_s}}\right) \approx \begin{cases} 0 & if \quad T \leq T_o \\ \frac{\widehat{T_s}-T_o}{T_m-T_o} exp(-\frac{Q}{RT_m}) & if \quad T > T_o \end{cases} \tag{4.22}$$

Where T_m is the melting temperature and T_o is obtained by intersecting the x-axis of Figure (4.3) with the tangent to the curve at the point of T_m, thus the following expression is obtained:

$$T_o = T_m\left(1 - \frac{RT_m}{Q}\right) \tag{4.23}$$

In this way, Equation (4.21) is reformulated using power laws as the following:

$$\frac{3}{2}\frac{\omega a}{\widehat{\delta}} \approx AB\left(\frac{\widehat{\tau_c}}{\tau_R}\right)^n \frac{\Delta\widehat{T_s}}{\Delta T_m} \tag{4.24}$$

Where $\Delta\widehat{T_s} = \widehat{T_s} - T_o$, $\Delta T_m = T_m - T_o$, and $B = exp(-Q/RT_m)$. Being ΔT_m and B known quantities from the material properties.

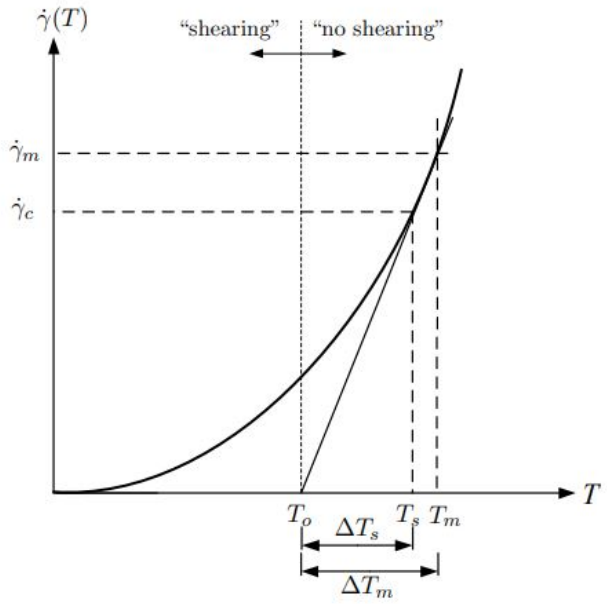

Figure 4.3: Asymptotic regimes for the constitutive behavior of the base plate.

4.1.4. Heat conduction outside the shear layer

Heat is transferred by conduction into the base plate outside the shear layer. The analysis of heat transfer in this region establishes a relationship between the characteristic temperature T_o and the tool traveling speed. The decoupling of the model into an inner and outer region allows setting different thermal boundary conditions on the base plate, including conduction cooling to the backing plate, convecting cooling to the atmosphere, and the existence of secondary heat sources.

Regardless of the chosen boundary conditions, the postulation of a slow-moving heat source guarantees that the isotherms belonging to the shear layer are circular and concentric to the pin axis. For this model, Rosenthal's thin plate solution based on a line heat source will be used [17, 21]. This solution estimates that heat transfer only occurs on the plane of the plate, neglecting the heat losses through conduction to the backing plate and convection to the atmosphere. On this side, Rosenthal's solution works with the assumptions of constant material properties and uniform initial temperature temperature T_∞, and is given by the following equation:

$$T(x') - T_p = \frac{q_l}{2\pi k_o} exp\left(-\frac{Vx'}{2\alpha}\right) K_o\left(\frac{Vr}{2\alpha}\right) \tag{4.25}$$

Where q_l is the intensity of the line heat source, k_o is the heat conductivity of the plate at $T = T_o$, and K_o is the modified Bessel function of a second kind and order 0. The coordinates x' and r correspond to a distance in the direction of travel and a radial distance from the line heat source respectively. In this way, the intensity of the heat source is given by:

$$q_l = \eta \text{ (torque/thickness) x (angular velocity)} = \eta(\tau 2\pi a^2)\omega \tag{4.26}$$

Where η is the total heat efficiency of the process. On the other hand, the radius of the isotherm corresponding to the shear layer is $r = r_0 = a + \delta$ but for a thin shear layer it can be approximated to r=a. Furthermore, since the Pe number is small, the expression $exp(-Vx'/2\alpha)$, from Equation (4.25) can be approximated to 1, and as Figure (4.4) illustrates, $K_o(Pe)$ increases when Pe decreases. With all the above, Equation (4.25) turns into the following:

$$\Delta T_o = T_o - T_\infty = \eta \frac{\omega a^2 \widehat{\tau}_c}{k_o} K_o(Pe) \tag{4.27}$$

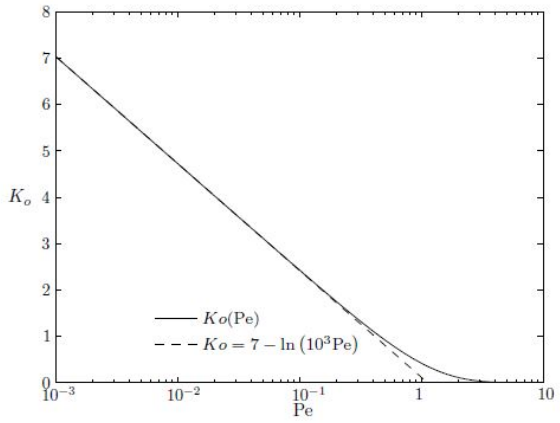

Figure 4.4: Behavior of the Bessel function Ko(Pe) and the asymptotic linearization valid for small Pe numbers (dashed line).

It is worth mentioning that Equation (4.27) suffers a modification based on Salazar's work. In previous versions of the model [22] it was considered that the heat loss through convection and conduction from the bottom and top of the plate was negligible since FSW is considered a low heat welding process, compared to other kinds of welding.

Furthermore, heat loss through the plate is expressed as:

$$\frac{h + h'}{k_o d} \tag{4.28}$$

Where h and h' are the coefficients of heat loss by convection and conduction of the top and bottom of the plate and their respective values are 10[W/m^2 · K] and 10,000[W/m^2 · K] [23] for all the materials. Meanwhile 'd' is the thickness of the plate and k_o is the thermal conductivity associated with the temperature at the point where $x = \delta$.

Secondly, the heat loss through thermal diffusivity is represented as:

$$\frac{V^2}{4\alpha^2} \tag{4.29}$$

Finally, the reason between the previous expressions can be expressed as:

$$\lambda = \frac{h + h'}{k_o d} \Big/ \frac{v^2}{4\alpha^2} = \frac{4\alpha^2(h + h')}{k_o d v^2} \tag{4.30}$$

The work of Salazar [2] consisted in comparing λ for different materials, against the reason between the torque measured in the experiments M and the estimation made by the mathematical model $\widehat{M}$. The results proved that the expression λ takes values up to the order of 100, which means that the effect of the heat loss through the plate is relevant compared to the thermal diffusivity and must be incorporated into the model. In this way, the variable ξ

is introduced:

$$\xi = r\sqrt{\left(\frac{V}{2\alpha}\right)^2 + \frac{h+h'}{k_o t}} \tag{4.31}$$

From this, equation (4.27) transforms into the following:

$$\Delta T_o = T_o - T_\infty = \eta \frac{\omega a^2 \widehat{\tau_c}}{k_o} K_o(\xi) \tag{4.32}$$

4.1.5. Solutions of the system of scaled equations

By taking Equations (4.9) (4.13) (4.24) and (4.32), a system of equations is constituted to find the expressions for the characteristic values. From the mentioned system, $\widehat{\tau_c}$ can be solved without the rest of the equations, and on the other side, linear algebra is used to find $\widehat{\delta}$, $\widehat{\Delta T_s}$ and $\widehat{q_c}$, hence the characteristic values are the following:

$$\widehat{\tau_c} = \frac{k_o \Delta T_o}{\eta^2 K_o} \tag{4.33}$$

$$\widehat{\delta} = a\left[\frac{8}{3}\frac{\Delta T_m}{\eta_s AB}\left(\frac{\tau_R a^2}{k_o}\right)^n \left(\frac{\eta K_o \omega}{\Delta T_o}\right)^{n+1}\right]^{1/2} \tag{4.34}$$

$$\widehat{\Delta T_s} = \Delta T_m \left[\frac{3}{2}\frac{\eta_s}{AB\Delta T_m}\left(\frac{\eta K_o}{\Delta T_o}\right)^{n-1}\left(\frac{a^2\tau_R}{k_o}\right)^n \omega^{n+1}\right]^{\frac{1}{2}} \tag{4.35}$$

$$\widehat{q_c} = \frac{3}{4}\left[\frac{3}{2}\frac{AB\eta_s^3}{\Delta T_m}\left(\frac{1}{\tau_R}\right)^n \left(\frac{1}{\omega}\right)^{n+1}\left(\frac{k_o}{a^2}\right)^{n+2}\left(\frac{\Delta T_o}{\eta K_o}\right)^{n+3}\right]^{\frac{1}{2}} \tag{4.36}$$

Furthermore, from Equation (4.33) the expression for the torque of the pin is obtained:

$$\widehat{M} = 2\pi \widehat{\tau_c} a^2 t \tag{4.37}$$

4.2. Material Properties

4.2.1. Thermal and Mechanical Properties

The thermal and mechanical properties of all the materials are summarized in Table (4.1). The flow shear stress of reference, τ_R can be obtained through Equation (4.38):

$$\tau_R = \frac{\sigma_R}{\sqrt{3}} \tag{4.38}$$

This equation is based on the distortion energy theory or the Von Mises criterion in uniaxial tension and pure shear. It is believed that pure shear stress occurs in the process of FSW, and several authors use this simplification for their models [7, 9, 24, 25]. The normal

stress of reference σ_R is assumed to be the yield stress of the alloy and for each material, its values were obtained from the Metals Handbook [26] and other publications referenced in Table (4.1).

The thermal efficiency (η) varies between the materials analyzed. As specified by Lienert et al. [27], the thermal efficiency of aluminum alloys is 90 % and of AISI steels is 75 %. On the other hand, the thermal efficiency of AISI 304 is 50 %, according to Zhu et al. [28], according to Lienert et al. [29] the thermal efficiency of Ti-6Al-4V is 47 %, and the thermal efficiency of AZ31 is 90 %, specified by Ogawa et al. [30]. Additionally, the efficiency η_s is 100 % for all materials.

Related to the thermophysical properties (k, C_p, ρ) of the new materials, these have been obtained with the software $JmatPro$. However, as the values show in molar units, the molar mass of each material must be calculated and then, each value can be converted to SI units.

Table 4.1: Thermal and mechanical properties of the selected materials.

Material	$T_{solidus}$[K]	k[W/mK]	C_p[J/kg]	ρ[kg/m^3]	σ_R[MPa]	η_s[%]	η[%]	k_{inf}
Al1080	919 [31]	211	1,055	2,680	105 [32]	100	90	163 [33]
Al2024	775	185	1,100	2,670	103	100	90	162
Al2195	813 [34]	196 [35]	1,338 [35]	2,770 [35]	692	100	90	170
Al2198	813 ”	177	1,170	2,750	550 [36]	100	90	170
Al2199	813 ”	151	1,062	2,780	550 ”	100	90	170
Al2219	816	175	1,020	2,950	217	100	90	160
Al2524	820 [37]	177	1,051	2,820	210 [38]	100	90	120 [39]
Al5059	847 [40]	146.9 [40]	1,261.4 [40]	2,552.8 [40]	34.8 [40]	100	90	121
Al5083	847	139	1,190	2,523	214	100	90	121
Al6061	855	200	1,160	2,590	55.2	100	90	152
Al6082	853 [41]	179	1,087	2,710	60 [42]	100	90	152
Al7010	775 [43]	135	1,170	2,950	103	100	90	175 [44]
Al7020	916 [45]	148	1,250	2,900	103	100	90	175 ”
Al7050	761	180	861	2,827	103	100	90	180
Al7075	805	192	1,109	2,693	103	100	90	166.7
Al7136	761 [46]	115	1,010	3,150	382 [47]	100	90	155 [48]
IF	1,802 [49]	36	1,170	2,950	170 [50]	100	75	25
AISI 1012	1,693 [51]	34.3	900	7,330	185 [52]	100	75	25
AISI 1018	1,733 [53]	33.1 [54]	699 [54]	7,314 [54]	205	100	75	25
AISI 1035	1,653 [51]	31	700	7,250	270 [52]	100	75	25
AISI 304	1,673	33.5	720	7,350	290	100	50	20
SSA038	801 [55]	122	1,114	3,000	120 [56]	100	90	20 [57]
AZ31	856 [58]	144.3	1,446.3	1,696	171 [59]	100	90	145 [60]
Ti-6Al-4V	1,877	27	750	4,198	875	100	47	7 [61]

4.2.2. Zener-Hollomon law constants

As specified by Sellars and Tegart [62], the deformation mechanisms operating in hot working processes at low level of stress are described by:

$$\dot{\varepsilon} = A\left(\frac{\sigma}{\sigma_R}\right)^n exp\left(-\frac{Q}{RT}\right) \tag{4.39}$$

Where 'A', 'Q', and 'n' are constants. However, Equation (4.39) does not consider the behavior of the materials at high stresses. Consequently authors present an empirical constitutive equation appropriate for low and high level of stresses, which can correlate data over a wide range of strain rate.

$$\dot{\varepsilon}' = A\left[sinh\left(\frac{\sigma'}{\sigma_R}\right)\right]^{n'} exp\left(-\frac{Q'}{RT}\right) \tag{4.40}$$

Where A', Q', n' and σ_R are constants obtained from the hot deformation model of Dr.Tello [63]. To incorporate the effects of Equation (4.40) into Equation (4.39) it is needed to find a relationship between both of them by their constants, for this, the following procedure must be performed:

1. Take the linearized form of Equations (4.39) and (4.40):

$$ln(\dot{\varepsilon}) = lnA + nln\left(\frac{\sigma}{\sigma_R}\right) - \frac{Q}{RT} \tag{4.41}$$

$$ln(\dot{\varepsilon'}) = lnA' + n'ln\left[sinh\left(\frac{\sigma'}{\sigma'_R}\right)\right] - \frac{Q'}{RT} \tag{4.42}$$

2. Calculate the partial derivatives of $\ln(\dot{\varepsilon})$ respect to 1/T and $\ln(\sigma)$, for both equations presented in step 1:

$$\frac{\partial ln(\dot{\varepsilon})}{\partial 1/T} = -\frac{Q}{RT} \tag{4.43}$$

$$\frac{\partial ln(\dot{\varepsilon})}{\partial ln(\sigma)} = n \tag{4.44}$$

$$\frac{\partial ln(\dot{\varepsilon'})}{\partial 1/T} = -\frac{Q'}{RT} \tag{4.45}$$

$$\frac{\partial ln(\dot{\varepsilon'})}{\partial ln(\sigma')} = \frac{n'\sigma'}{\sigma'_R}\frac{1}{tanh(\frac{\sigma'}{\sigma'_R})} \tag{4.46}$$

3. Evaluate each equation introduced in step 2 at the solidus temperature of the material and at the average value of strain rate achieved during the process, which is $\dot{\varepsilon}$=300(s^{-1}). Finally, equating the respective partial derivatives:

$$\frac{Q}{RT} = \frac{Q'}{RT} \Rightarrow Q = Q' \tag{4.47}$$

$$n = \frac{n'\sigma'}{\sigma'_R} \frac{1}{tanh(\frac{\sigma'_R}{\sigma'})} \tag{4.48}$$

Where σ' is the shear stress calculated with Equation (4.41) at 300 (s^{-1}) and $T_{solidus}$. Thereby, 'Q' and 'n' can be calculated using (4.47) and (4.48) respectively.

Table (4.2) summarizes the constants obtained by using the described procedure. The values of A', n', Q' and σ_R', were obtained from Dr. Tello's thesis [22] for the original database, and in the case of the new materials, the values were obtained from a series of publications referenced in the following Table, as well as from values belonging to similar materials.

Table 4.2: Values of constants for the Zenner-Hollomon constitutive Equations (4.39) and (4.40).

Material	A'[s^{-1}]	n'	Q'=Q[kJ/mol]	σ'_R[MPa]	A[s^{-1}]	n
Al1080	1.37 x 10^{11} [64]	3.97 [64]	232 [64]	36.8 [64]	1.81 x 10^{15}	11.93
Al2024	2.29 x 10^{11}	5.46	178	47.7	6.52 x 10^{14}	11.50
Al2195	2.29 x 10^{12}	2.38	162	293.0	1.73 x 10^{12}	3.54
Al2198	2.29 x 10^{12}	2.38	162	293.0	2.93 x 10^{13}	3.37
Al2199	2.29 x 10^{12}	2.38	162	293.0	2.93 x 10^{13}	3.37
Al2219	1.37 x 10^{11} [65]	6.65 [65]	160 [65]	68.0 [65]	1.74 x 10^{16}	10.08
Al2524	1.37 x 10^{11} "	6.65 "	160 "	68.0 "	1.64 x 10^{16}	10.01
Al5059	1.64 x 10^{10}	2.44	173	34.8	3.84 x 10^{8}	8.46
Al5083	1.64 x 10^{10}	2.44	173	34.8	1.78 x 10^{15}	8.44
Al6061	1.63 x 10^{13}	5.33	191	60.7	1.72 x 10^{13}	7.68
Al6082	1.63 x 10^{13}	5.33	191	60.7	3.28 x 10^{13}	7.71
Al7010	5.04 x 10^{19} [66]	0.99 [66]	347 [66]	11.4 [66]	2.23 x 10^{22}	15.87
Al7020	5.04 x 10^{19} "	0.99 "	347 "	11.4 "	1.91 x 10^{23}	8.29
Al7050	1.45 x 10^{10}	3.39	165	56.6	6.48 x 10^{13}	10.70
Al7075	5.34 x 10^{8}	3.47	160	33.9	1.74 x 10^{12}	11.95
Al7136	5.34 x 10^{8}	3.47	160	33.9	2.13 x 10^{19}	12.61
IF	5.60 x 10^{12} [67]	5.8 [67]	285 [67]	113.6 [67]	3.12 x 10^{14}	6.20
AISI 1012	2.36 x 10^{13}	4.32	371	56.6	6.87 x 10^{16}	6.84
AISI 1018	2.36 x 10^{13}	4.32	371	56.6	6.95 x 10^{16}	5.67
AISI 1035	2.36 x 10^{13}	4.32	371	56.6	1.06 x 10^{17}	5.89
AISI 304	1.62 x 10^{16}	4.69	441	119.0	4.36 x 10^{18}	5.51
SSA038	5.34 x 10^{8}	3.47	160	33.9	1.64 x 10^{12}	12.07
AZ31	1.78 x 10^{9} [68]	4.90 [68]	136 [68]	83.3 [68]	8.47 x 10^{11}	8.01
Ti-6Al-4V	3.37 x 10^{8}	3.39	231	47.9	3.96 x 10^{14}	4.63

Chapter 5

Results

In order to compare the estimations to the measurement and numerical results, the ratio of measurement and numerical results to estimations ($X/\widehat{X}$) is introduced, with the above, two ratios are stablished: maximum temperature ratio and torque ratio, which can be obtained by Equations (4.35) and (4.37) respectively. In this way, the ratios are expressed as it follows:

$$\theta = \frac{T_s - T_\infty}{\widehat{T_s} - T_\infty} \tag{5.1}$$

$$\frac{M}{\widehat{M}} \tag{5.2}$$

It can be noticed that there is no ratio made for the volumetric heat $\widehat{q_c}$ because there are not appropriate techniques for its measurement. In the same way, the measurements of $\widehat{\delta}$ are not accurate enough to make a comparison to the estimations. On the other hand, the hat symbol refers to the estimations made by the model, while the symbol without hat refers to the the measurement and numerical results present in the literature.

To make the comparison, each ratio is plotted against the four simplifications presented in Equations (2.1), (2.2), (2.3) and (2.4). If the ratios happen to be constant near one, i.e. the graph presents values near one on the 'Y' axis, the estimations made by the model manage to capture the proper order of magnitude of the target variable. On the other side, if the ratio moves away from the asymptotic regime, this implies that the simplifications become relevant and a correction function must be applied. The latter allows the estimations to reach values that are closer to the measurements and numerical results, by taking into account the forces neglected in the formulation of the scaling law.

It is worth mentioning that the improvements cannot suppress the experimental or numerical error, and the scatter in the comparison of the improved scaling laws to experiments or calculations is unavoidable.

The correction function is defined as follows:

$$f\left(Pe, \frac{\widehat{\delta}}{a}, \frac{V}{\omega\widehat{\delta}}, \frac{T_p - T_\infty}{\widehat{T_s} - T_\infty}\right) = C_1(1 + C_2 Pe)^{C_3}\left(1 + C_4\frac{\widehat{\delta}}{a}\right)^{C_5}\left(1 + C_6\frac{V}{\omega\widehat{\delta}}\right)^{C_7}\left(1 + C_8\frac{T_p - T_\infty}{\widehat{T_s} - T_\infty}\right)^{C_9} \tag{5.3}$$

Where C_i (i = 1, 2, ..., 9) are constants fitted using a minimum least squares regression given by the following:

$$\Phi = Min\sum_{i}^{n}\left(log\left(\frac{X}{\widehat{X}}\right)_i - log(f_i)\right)^2 \tag{5.4}$$

Where n is the total number of data considered. In case all the simplifications are neglected, the constant C_1 accounts for mathematical errors induced by the scaling model. In case any of the simplifications become dominant, the coefficients that go with the respective simplification capture a power law behavior. Thus, the improved estimations are given by the following:

$$\widehat{X}^+ = \widehat{X} \cdot f\left(Pe, \frac{\widehat{\delta}}{a}, \frac{V}{\omega\widehat{\delta}}, \frac{T_p - T_\infty}{\widehat{T_s} - T_\infty}\right) \tag{5.5}$$

Since each simplification has a different contribution to the total error of the model, it is worth mentioning that in this work only the most influential simplifications will be considered in the regression that allows to obtain the improved estimation. Each selected simplification will be justified in the next section. This work will analyze two types of graphs. In the first place, there are the graphs that compare the ratio ($X/\widehat{X}$) against a simplification. Related to the used data, there will be used the tests that fulfill all the simplifications except the one that is being used as the horizontal axis, and those experiments that use a Trivex-type pin. On the other hand, there are the graphs that compare the estimations (with and without the improvement $\widehat{X}^+$) to the measurement and numerical results (X), for these cases, all the data available is considered. In this way, the graphs made are the ones that compare the estimations of the model to the measurement and numerical results for the maximum temperature and torque. In appendices A and B the compiled data and the results of the estimations can be found.

5.1. Estimation of the maximum temperature

Figure (5.1) presents the ratio of maximum temperature as a function of the Pe number given by Equation (2.1). It can be observed that the simplification is always satisfied since Pe<1 for all the tests and the ratio of maximum temperature remains around a band that is defined by the trendline given by Equation (5.6). Additionally, the range of the ratio θ is between 0.34-1.01, except for Benavides et al. Al2024 [69] which is near 0.25, and the graph counts with 31 experiments and 74 tests.

Figure (5.2) presents the ratio of maximum temperature as a function of $\widehat{\delta}/a$. It is observed that this simplification is not always satisfied. Additionally, a systematic deviation from the asymptotic regime can be observed for values of $\widehat{\delta}/a>1$. The above implies that this simplification influences the results and it is necessary then to involve its effect on the estimation of the maximum temperature. The figure presents a range of the ratio θ between 0.1-1.01, with 38 experiments and 84 tests.

Figure (5.3) presents the ratio of maximum temperature as a function of $\mathrm{V}/\omega\widehat{\delta}$. It is observed that this simplification is not always satisfied, even reaching values close to the order of 10^6. Nevertheless, the ratio of maximum temperature remains almost constant in the range of study and remains around a band defined by the trendline described by Equation (5.6). The graph presents a range of the ratio θ between 0.34-1.1 (except for Benavides et al. Al2024 [69] which is near 0.25), with 50 experiments and 150 tests.

Figure (5.4) presents the ratio of maximum temperature as a function of $T_p - T_\infty/\widehat{T_s} - T_\infty$. It is observed that this simplification is not always satisfied but the ratio of maximum temperature falls around a band defined by the trendline described by Equation (5.6). The graph presents a range of the ratio θ between 0.34-1.01 (except for Benavides et al. Al2024 [69] which is near 0.25), with 31 experiments and 86 tests.

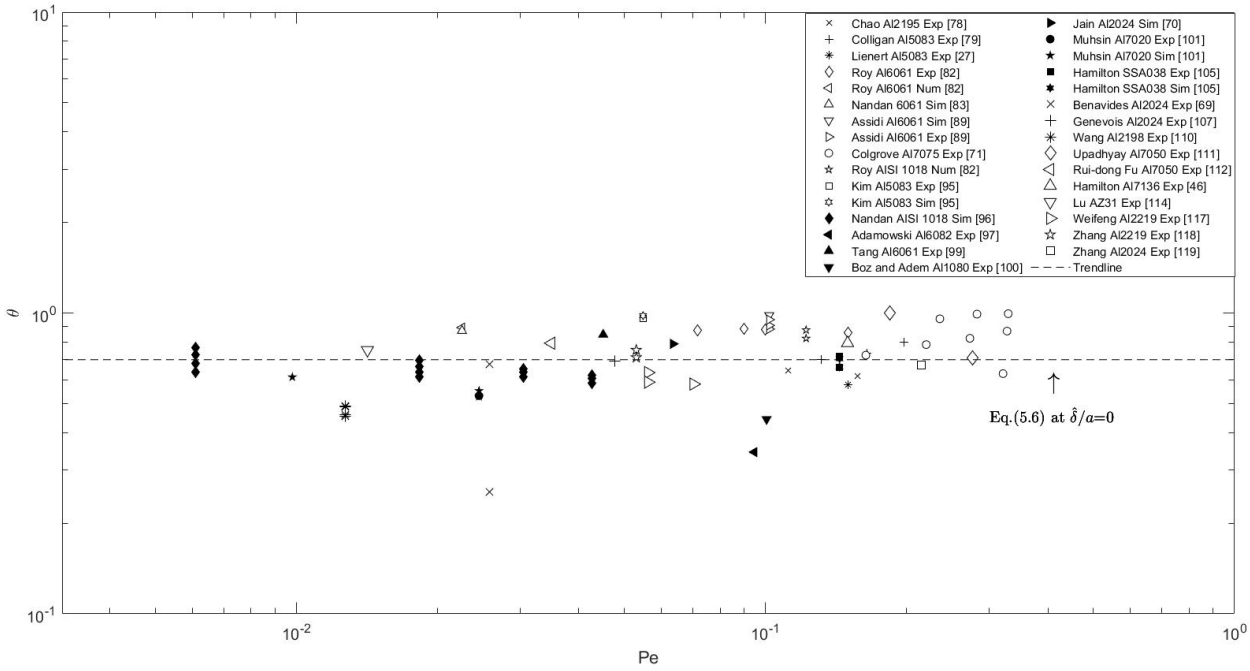

Figure 5.1: Comparison between the ratio of maximum temperature as a function of Pe.

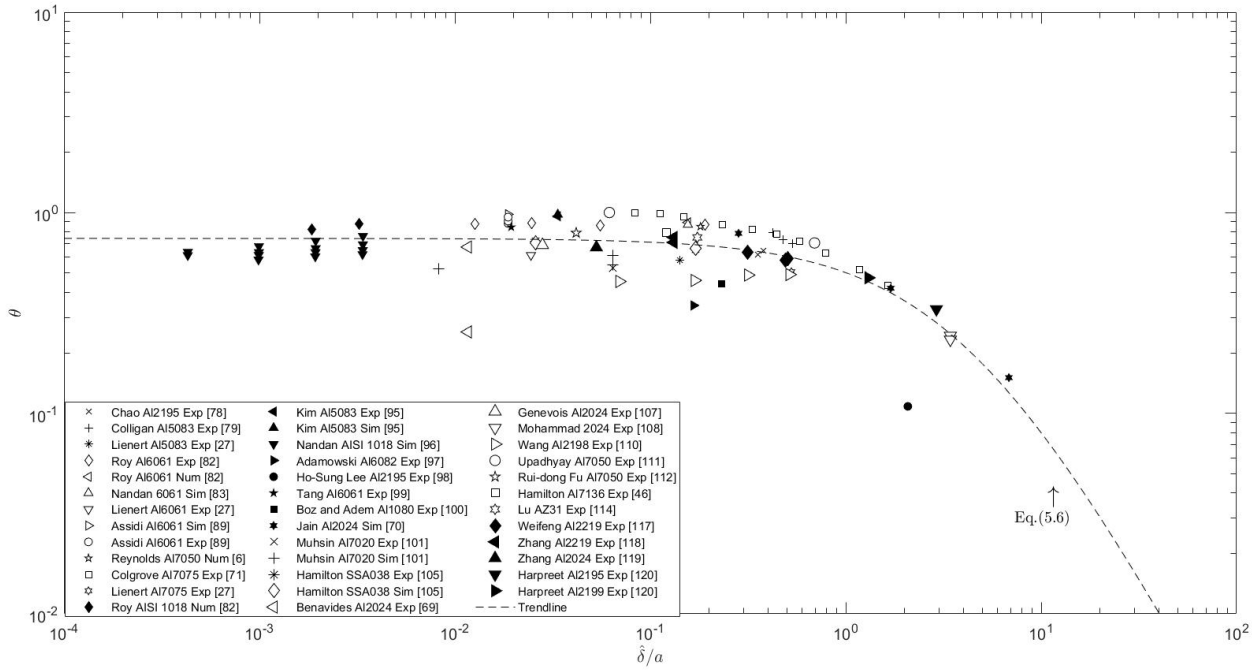

Figure 5.2: Comparison between the ratio of maximum temperature as a function of $\widehat{\delta}/a$.

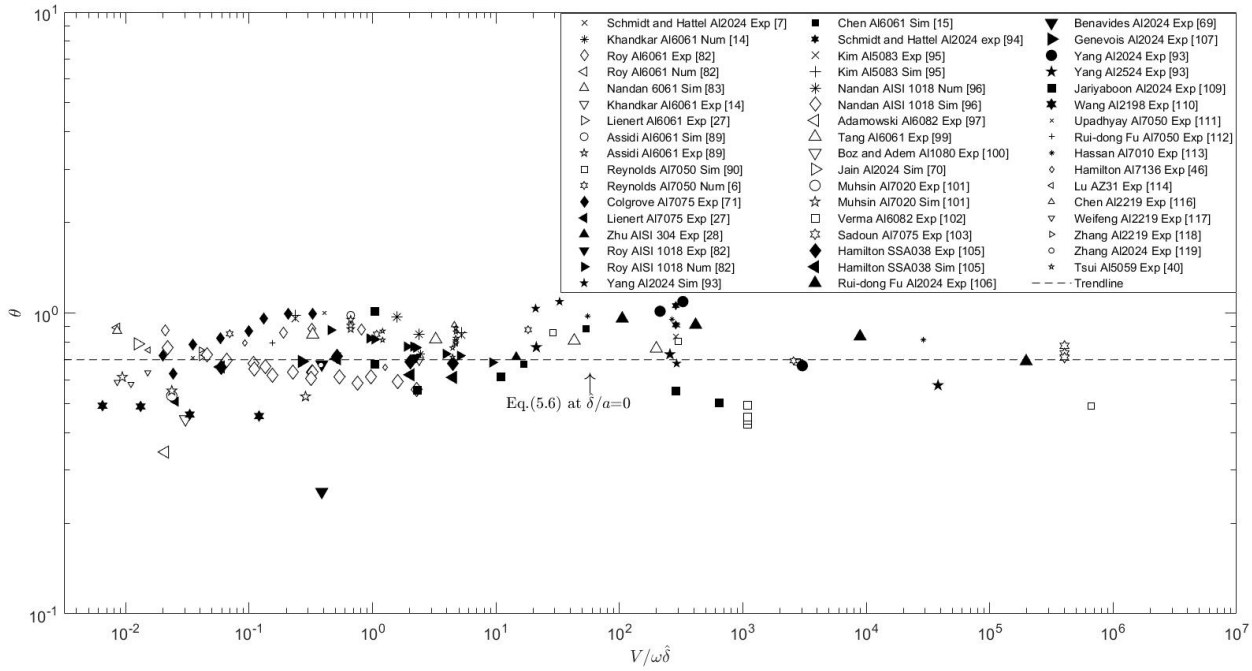

Figure 5.3: Comparison between the ratio of maximum temperature as a function of $\mathrm{V}/\omega\widehat{\delta}$.

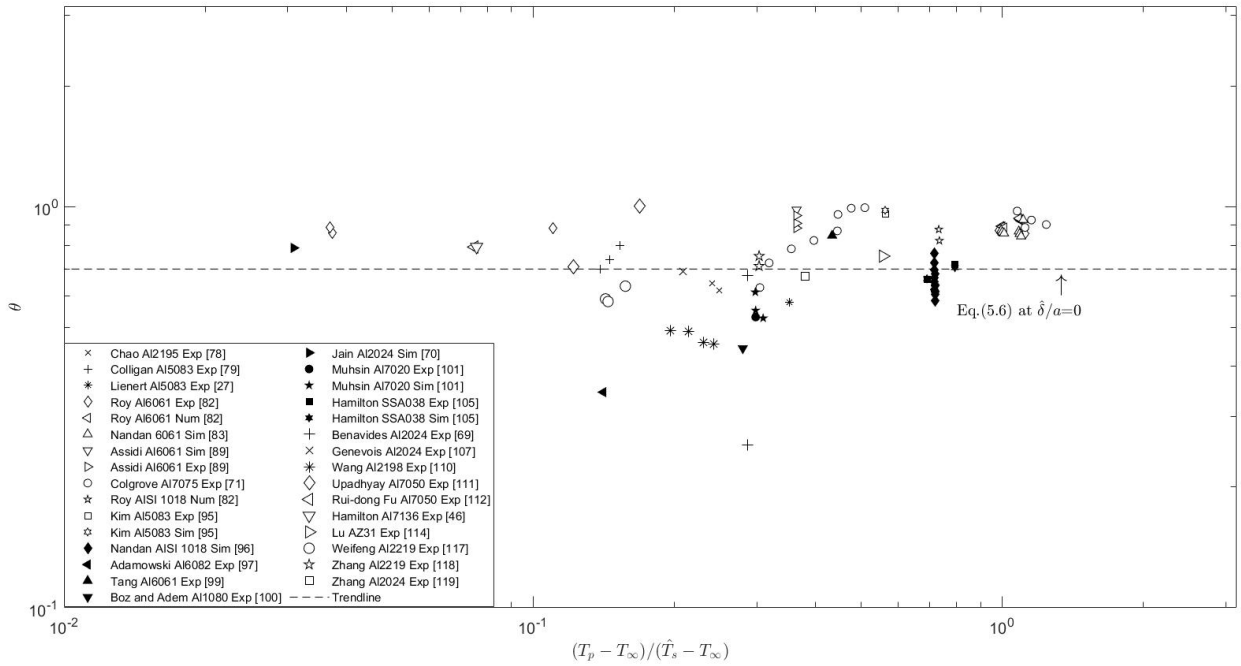

Figure 5.4: Comparison between the ratio of maximum temperature as a function of $T_p - T_\infty / \widehat{T_s} - T_\infty$.

The average error associated to the estimation of maximum temperature is 30.3 % and as the values of the estimations are in most of the cases higher than the measurement and numerical results, it can be said that the model overpredicts the temperature. To find the best correction function for the estimation of the maximum temperature it is required to study the error of the regression analysis (Equation (5.4)). For this task, three cases are analyzed:

1. Case 1: Only constant C_1 is considered.
2. Case 2: Only $\widehat{\delta}/a$ is considered.
3. Case 3: All the simplifications are considered.

Table (5.1) introduces the values of all the constants and the error for each case. Comparing Case 1 to Case 2, the error decreases by about 37 %, however, if Case 2 is compared to Case 3 the reduction of the error is much smaller (approximately 6 %). Therefore, Case 2 is considered the best correction function to improve the estimation of the maximum temperature.

Table 5.1: Summary of constants and error values of the correction functions for the estimation of maximum temperature.

	Case 1	Case 2	Case 3
C1	0.70	0.74	0.78
C2			0.37
C3			0.12
C4		0.24	0.28
C5		-1.82	-1.81
C6			0.83
C7			-0.02
C8			-0.09
C9			0.04
Error	22.13	13.92	13.06

Thus, the correction function is given by the following:

$$f\left(\frac{\widehat{\delta}}{a}\right) = 0.74\left(1 + 0.24\frac{\widehat{\delta}}{a}\right)^{-1.82} \tag{5.6}$$

In this way, the relation between the estimation of the maximum temperature and its improvement is given by:

$$(\widehat{T_s} - T_\infty)^+ = (\widehat{T_s} - T_\infty) \cdot f\left(\frac{\widehat{\delta}}{a}\right) \tag{5.7}$$

The trendlines presented in Figures (5.1), (5.3) and (5.4) correspond to the correction function evaluated at $\widehat{\delta}/a = 0$.

On the other hand, the following two figures illustrate the comparison of the measurement and numerical results $(T_s - T_\infty)$ to the estimation of the maximum temperature with and without the improvement (Figures (5.5 (a)) and (5.5 (b)) respectively).

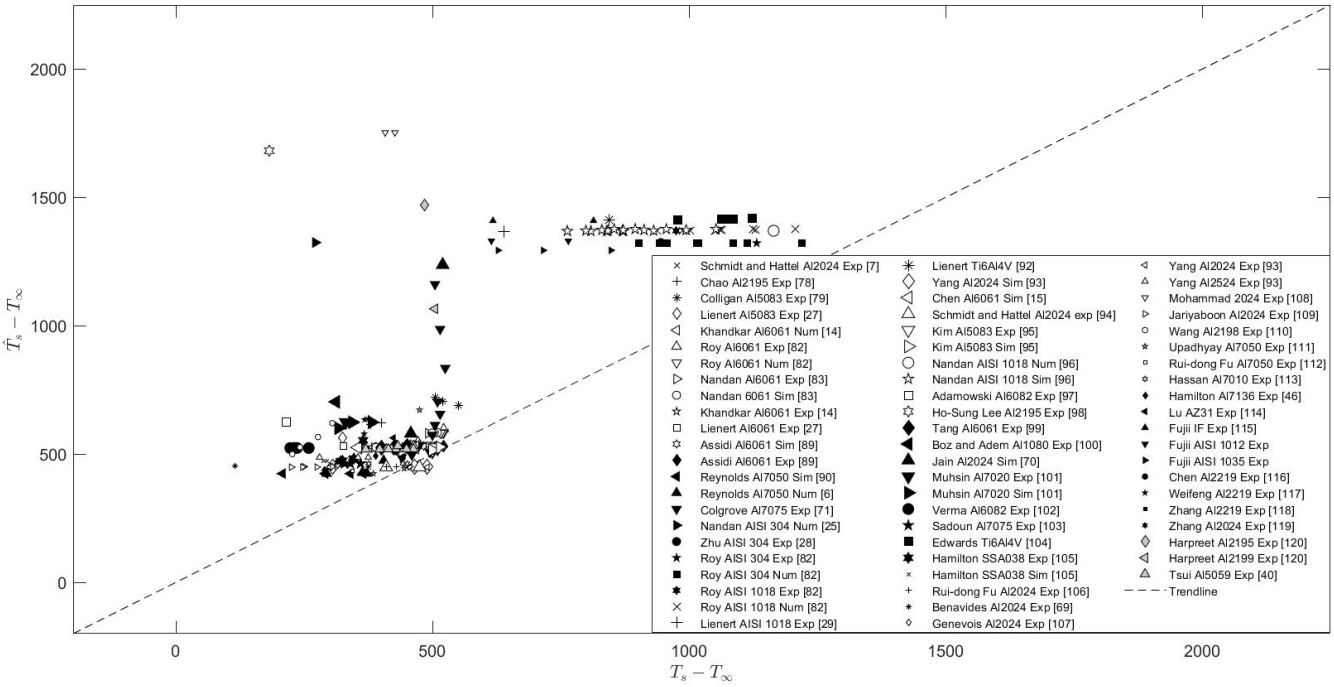

Figure 5.5(a): Correlation between the maximum temperature reported in the literature ($T_s - T_\infty$) and the estimation of the maximum temperature ($\widehat{T_s} - T_\infty$).

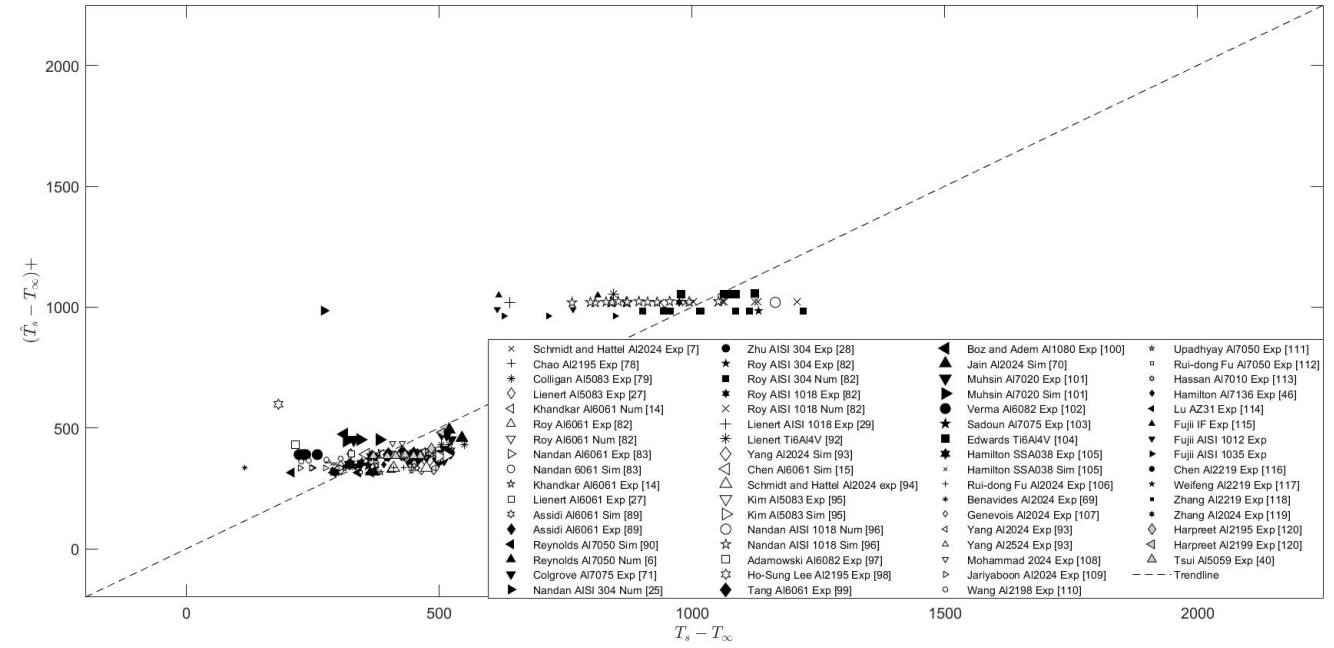

Figure 5.5(b): Correlation between the maximum temperature reported in the literature ($T_s - T_\infty$) and the improved maximum temperature $(\widehat{T_s} - T_\infty)^+$.

While Figure (5.5 (a)) shows that the correlation does not fall in the 1:1 line for most of the materials, Figure (5.5 (b)) shows that the correction function applied brings the data closer to the 1:1 trend. Furthermore, two clusters are observed: aluminum alloys are grouped at low temperatures, due to their lower melting temperature, and ferrous and titanium alloys at high temperatures, due to their higher melting temperature. Finally, the graphs present 66 experiments and 215 tests.

5.2. Estimation of Torque

Figure (5.6) presents the ratio of torque as a function of Pe number (Equation (2.1)). It is observed that in this case, the simplification is always satisfied (with $Pe<1$ for all the materials), and the ratio of toque presents a slight increasing tendency as Pe increases. The graph presents 9 experiments and 42 tests, and the ratio of torque remains in the range of 0.24-1.0, except for the experiment of Lienert et al. Al7075 Exp [27], which is near 2.7.

Figure (5.7) presents the ratio of torque as a function of $(\widehat{\delta}/a)$. Although the simplification is not always satisfied, the ratio of torque remains almost constant in the range of study and falls around a band defined by the trendline obtained with Equation (5.8). The graph presents 10 experiments and 51 tests, and the ratio of torque remains in the range of 0.4-1.2, except for the experiments of Jain et al. Al2024 [70] which reach values near 0.24.

Figure (5.8) presents the ratio of torque as a function of $(\mathrm{V}/\omega\widehat{\delta})$. Despite the simplification is not always satisfied, with results reaching values of $\mathrm{V}/\omega\widehat{\delta}$ of around 10^6, the ratio of torque remains almost constant in the range of study and falls around a band defined by the trendline obtained with Equation (5.8). The graph presents 16 experiments and 96 tests, and the ratio of torque remains in the range of 0.24-1.24.

Figure (5.9) presents the ratio of torque as a function of $T_p - T_\infty/\widehat{T_s} - T_\infty$. It is observed that this simplification is always satisfied, with the exception of three tests from Colgrove and Shercliff Al7075 [71]. The ratio of torque falls around a band defined by the trendline described by Equation (5.8). The graph presents a range of the ratio θ between 0.24-1.2, (except for Lienert et al. Al7075 Exp [27] which is near 2.7), with 11 experiments and 49 tests.

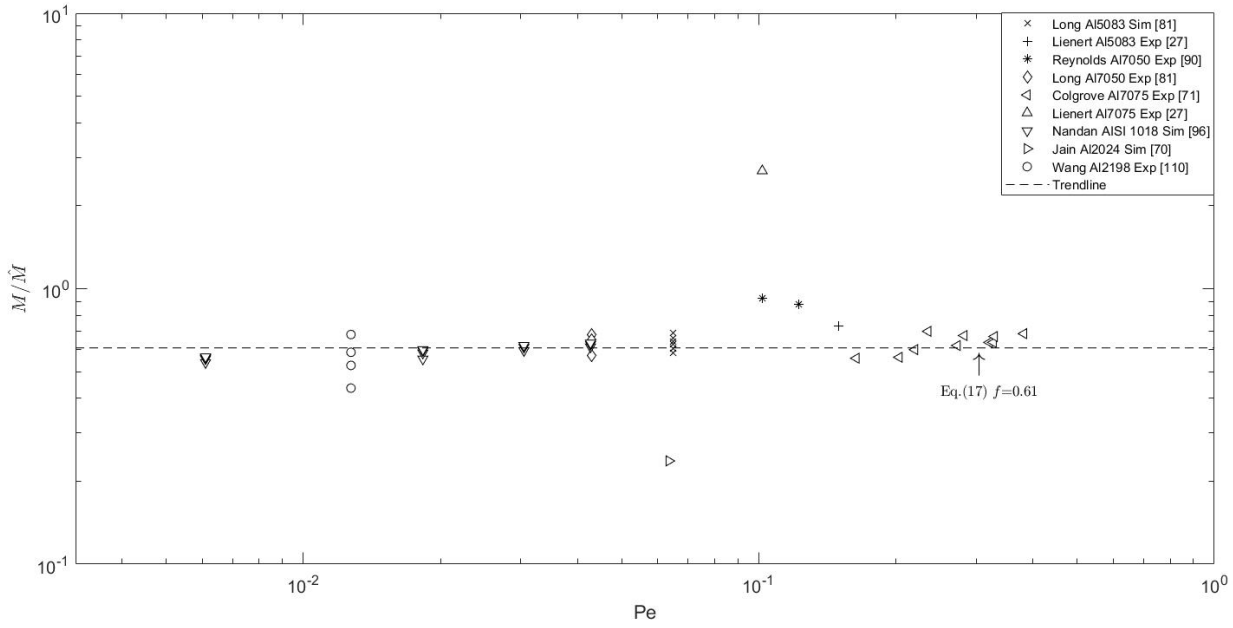

Figure 5.6: Comparison between the ratio of torque as a function of Pe.

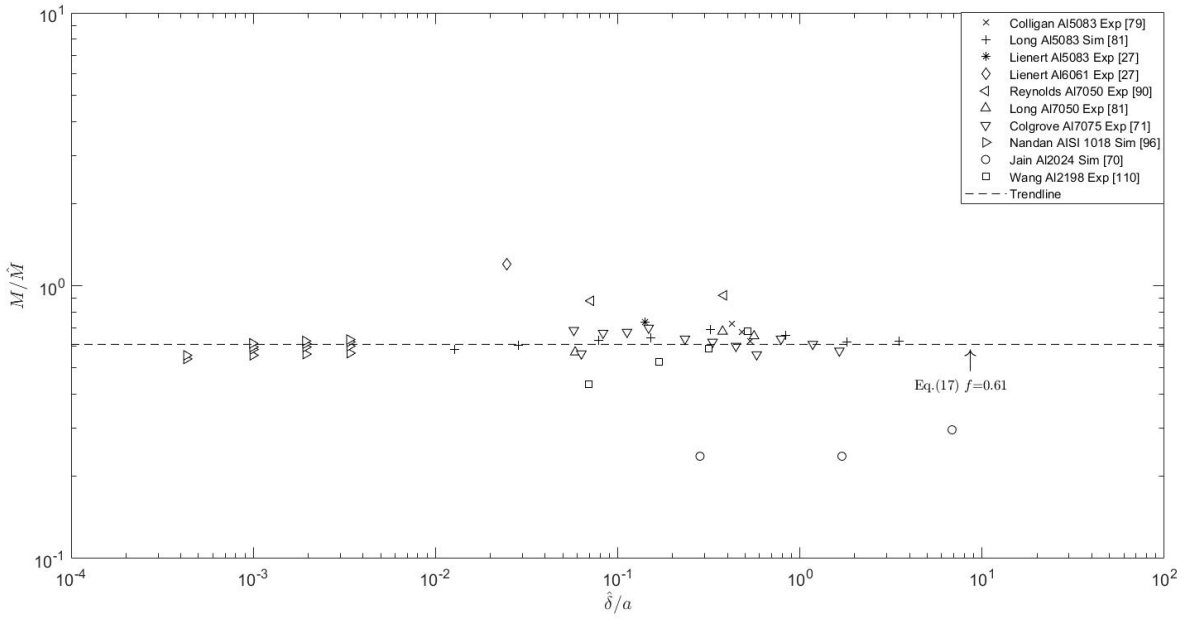

Figure 5.7: Comparison between the ratio torque as a function of $\widehat{\delta}/a$.

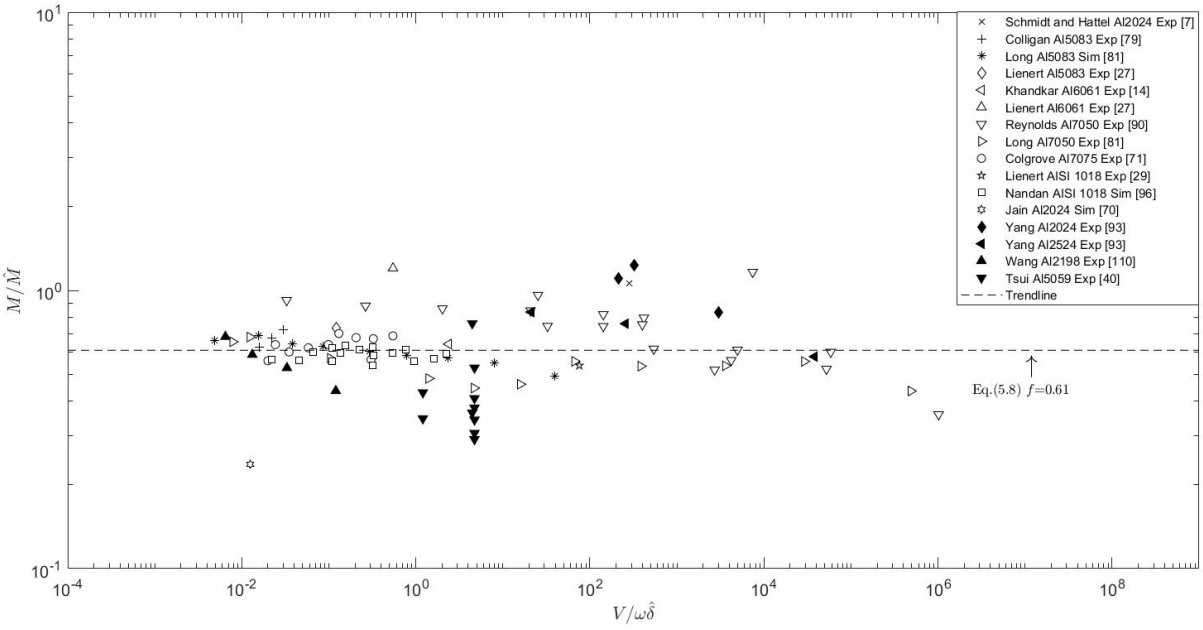

Figure 5.8: Comparison between the ratio of maximum temperature as a function of V/$\omega\widehat{\delta}$.

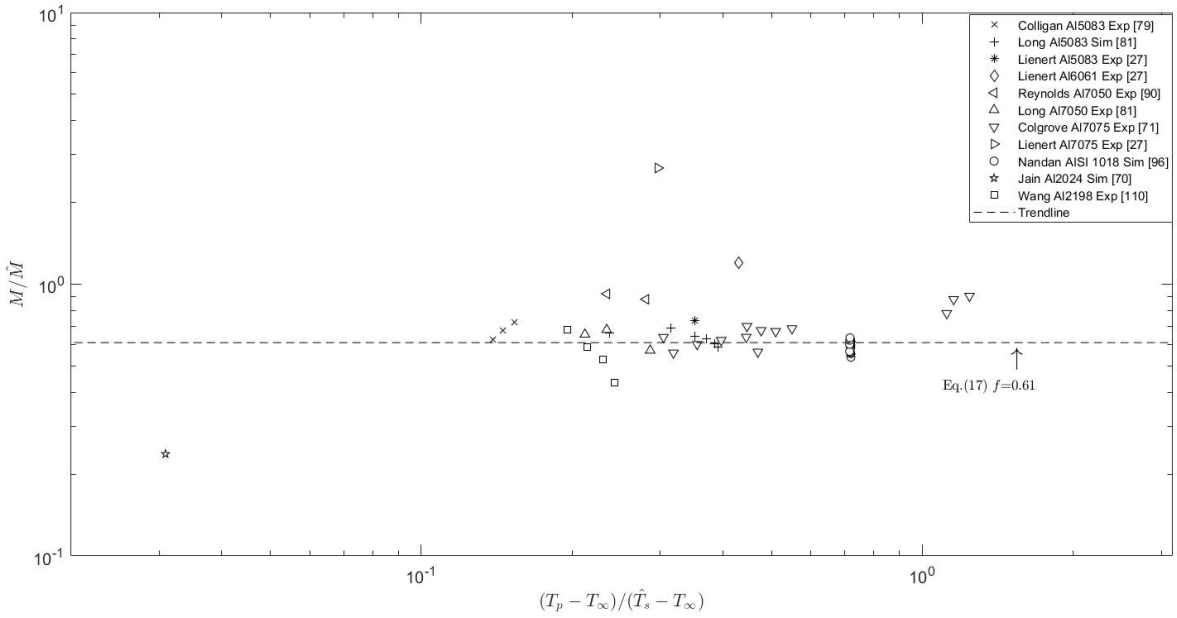

Figure 5.9: Comparison between the ratio of torque as a function of $T_p - T_\infty/\widehat{T_s} - T_\infty$.

The average error associated to the estimation of torque is 76 % and as the values of the estimations are in most of the cases higher than the measurement and numerical results, it can be said that the model overpredicts the torque.

To determine the best correction function for the estimation of torque it is necessary to study the error of the regression analysis (Equation (5.4)). For this study, three cases are analyzed :

- Case 1: only the constant C_1 is considered.
- Case 2: Only Pe is considered.
- Case 3: All the simplifications are considered.

Table (5.2) presents the results of the constants and errors obtained. By comparing Case 1 to Case 2 and even existing a slight trend related to Pe number, the error decreases by approximately 1 % which suggests that Case 1 can provide a correction function almost as satisfactory as Case 2. Comparing Case 1 to Case 3, the error decreases by approximately 6 %. This is not an important reduction, considering all the coefficients involved in the correction function. In this way, Case 1 can capture the overall non-dependence between the ratio of torque and the simplifications.

Table 5.2: Summary of constants and error values of the correction functions for the estimation of maximum torque.

	Case 1	Case 2	Case 3
C1	0.61	0.38	0.53
C2		-0.62	-0.10
C3		0.51	-0.14
C4			0.01
C5			-3.51
C6			0.71
C7			0.00
C8			1.17
C9			0.38
Error	11.89	11.75	11.12

Therefore, the correction function can be expressed by a unique constant value which is given by:

$$f = 0.61 \tag{5.8}$$

In this way, the relation between the estimation of torque and its improvement is given by:

$$\widehat{M}^{+} = 0.61 \cdot \widehat{M} \tag{5.9}$$

The following figures illustrate the comparison of the measurement and numerical results (M) to the estimation of the torque with and without the improvement (Figures (5.10 (a)) and (5.10 (b)) respectively):

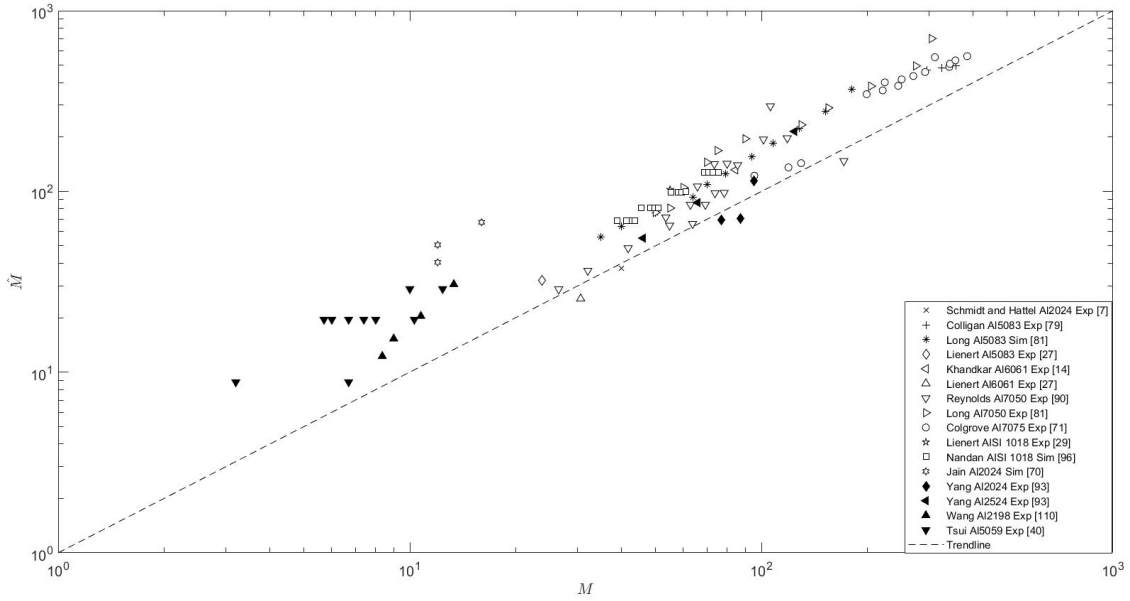

Figure 5.10 (a): Correlation between the torque reported in the literature (M) and the estimation of torque ($\widehat{M}$).

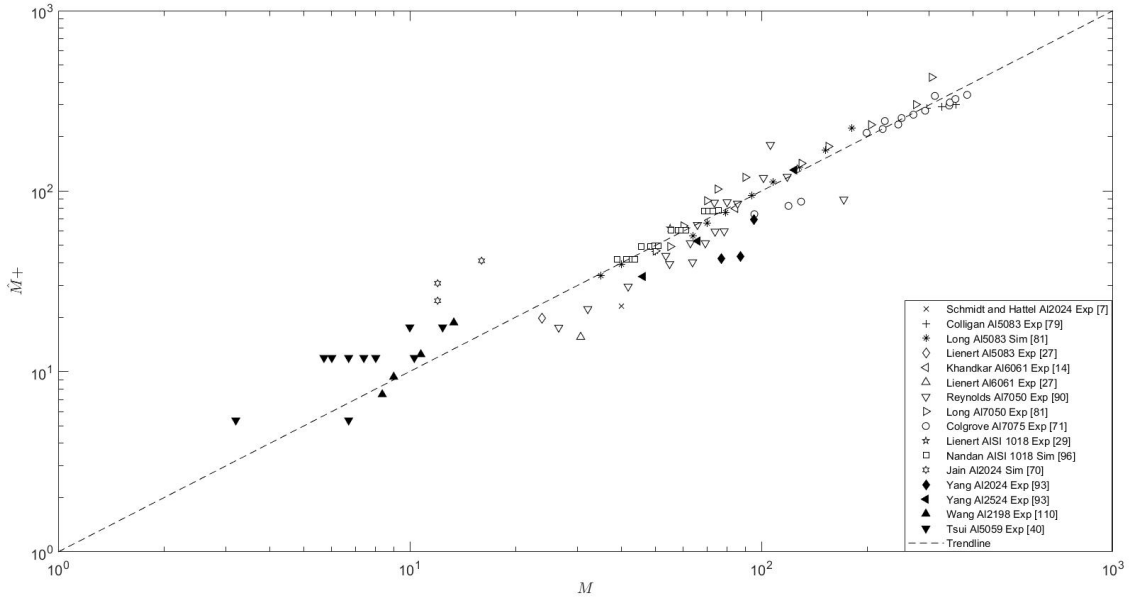

Figure 5.10 (b): Correlation between the torque reported in the literature (M) and the improved torque ($\widehat{M}$).

While Figure (5.10 (a)) shows that the correlation mostly does not fall in the 1:1 line, Figure (5.10 (b)) shows that the correction function applied brings the data closer to the 1:1 trend. Finally, the graphs present 16 experiments and 103 tests.

Chapter 6

Discussion

The estimation of maximum temperature is analyzed with θ (see Equation (5.1)) which is the ratio between $(T_s - T_\infty)$ and $(\widehat{T_s} - T_\infty)$. In the case of Figure (5.1), it can be seen that the results of temperature ratios are close to 1 (approximately 0.73), which means that the values of maximum temperature at the pin/shear layer interface predicted by the model approach to the measurement and numerical results, this occurs independently of the value of Pe, and additionally, the assumption $Pe<1$ is satisfied for all the tests, which allows to affirm that Pe does not influence the result of θ.

It can be observed in Figure (5.2), that starting from $\widehat{\delta}/a \approx 0{,}1$, the values of θ begin to decrease, deviating the ratio of its asymptotic regime which implies that the simplification influences the estimation of maximum temperature, and therefore, it is necessary to consider it in the correction function to improve the estimation of maximum temperature. Even though the error of the regression analysis (see Table (5.1)) is not much smaller than the case that does not consider the simplification from Equation (2.2), it is still a lower error and in Figure (5.2) it can be seen that the trend fits the data, which means that the consideration of the simplification in the correction function, aims to capture the errors introduced during the generation of the model.

It is worth mentioning that the tests of the the material AISI1018 are at the left side of the graph, which is due to the fact that steels have a higher density and therefore the shear layer thickness is lower. This happens because these materials have a higher viscosity, thus their resistance to deformation is higher, resulting in a thinner shear layer and a lower temperature of the process, producing then, a lower measured maximum temperature than the estimated maximum temperature.

In the case of Figure (5.3), as well as the case of Figure (5.4), the results of temperature ratio are close to 1, which means that predictions made by the model approach to the measurement and numerical results, even in the case when multiple experiments do not accomplish the assumptions plotted on the 'X' axis. Additionally, it can be observed that a

higher number of experiments are present in Figure (5.3) since the simplification of Equation (2.3) restricted more experiments than the other simplifications, this occurs because this simplification is more often bigger than one as a result of a lower shear layer thickness estimation.

In all the figures that plot against the temperature ratio, it can be noticed that the experiment from Benavides et al. Al2024 [69] stays away from the trend, this occurs because the predicted maximum temperature (750 (K^o)) is much higher than the experimental one (413 (K^o)). This difference occurs because the result of the predicted temperature has a high dependency on the temperature at the shear layer/base plate interface (T_o), which in turn depends on the melting temperature of the base plate (T_m), which is characteristic of the base material. As a result, it can be said that the predicted maximum temperature ($\widehat{T_s}$) depends on the melting temperature, which is higher than the actual maximum temperature (T_s), this is a correct statement, since in FSW melting does not occur. However, the maximum temperature reached must be high enough to deform the material. In the case of Benavides et al. Al2024 [69], the fact that the experimental maximum temperature is much lower than the predicted maximum temperature, and thus, lower than the melting temperature, means that the actual process did not need, in fact, such a high temperature to deform the material, or that there was an error at the measurements.

Finally, the fact that in Figures (5.1), (5.3) and (5.4) the temperature ratio is close to 1 along the entire 'X' axis, could lead to say that the maximum temperature manages to be properly predicted by the model estimations. However, there is the case of Figure (5.2), in which, at is mentioned previously, simplification (2.2) has a significant influence on the estimation of maximum temperature. Thus, to tune the estimation, a correction function dependent on the mentioned simplification is proposed.

The effect of the correction function on the maximum temperature estimation can be observed by comparing Figures (5.5 (a)) and (5.5 (b)), since in the first one, the data is mostly found above the trendline of 1:1, which implies that the predicted maximum temperatures are higher than their respective measurements, while in Figure (5.5 (b)) it is observed that the groups of experiments manage to focus around the 1:1 trendline, which indicates that the correction factor provides accuracy to most of the estimations. It can be noticed as well that in both graphs the data tends to separate in aluminum alloys (with lower melting temperature) and steel ones (with higher melting temperature), and in the case of steels, when the maximum temperature increases, the estimation does not.

There exist particular cases of experiments that, including the correction function, remain away from the 1:1 trendline. In first place, there is the case of Nandan et al. AISI 304 [**?**], which has a temperature difference ($T_s - T_\infty$) of 272(K^o) compared to the difference when applying the correction function to the estimation $(\widehat{T_s} - T_\infty)^+ = 985(K^o)$, this occurs, as well as in the Benavides et al. Al2024 [69] case, because the temperature that achieves the

deformation of the base material in this test is much lower than the melting temperature characteristic of the material, which by having a high influence in the value of the maximum predicted temperature, produces this wide difference between the values of $(T_s - T_\infty)$ and $(\widehat{T_s} - T_\infty)^+$. However, it is worth mentioning that the correction function manages to bring the temperature differences closer than in the case without the correction ($\widehat{T_s} - T_\infty =$ 1,324(K°)). A similar case is the experiment of Ho-Sung Lee et al. Al2195 [98], in which the difference $(T_s - T_\infty)$ has a value of 182(K°), compared to $(\widehat{T_s} - T_\infty)^+$=611(K°). This occurs because the parameter of rotation speed of the tool ω is higher for this experiment (600 r.p.m), compared to the rest of the experiments of the material Al2195 (around 200 r.p.m). Although this difference is not exorbitant, the value of predicted maximum temperature $\widehat{T_s}$ is very sensitive to variations in the rotational speed of the tool, and with minor alterations of this parameter, there may be significant changes in the result of $\widehat{T_s}$. In Figure (5.6), it can be seen a slight increase of the $M/\widehat{M}$ ratio, as Pe increases. This means that a bigger translation velocity produces a $M/\widehat{M}$ ratio closer to 1, and the difference between the estimations and the measurements decreases.

It can be observed in Figures (5.7) and (5.8) that he ratio $M/\widehat{M}$ is close to 1 and remains relatively constant in the range of validity of the simplifications, even when the assumption plotted on the 'X' axis is not accomplished. Whereby it can be said that there is no dependency between $M/\widehat{M}$ and $\hat{\delta}/a$ or between $M/\widehat{M}$ and $\mathrm{V}/\omega\hat{\delta}$. In the case of figure (5.7), it can be noticed that steels are found in the left half of the graph as well as it was seen previously in Figure (5.2). On the other side, it is observed that Figure (5.8) has more experiments that the rest of the torque graphs. This occurs for the same reason why Figure (5.3) presented a higher number of samples.

Related to Figure (5.9), it can be observed a $M/\widehat{M}$ ratio that remains relatively constant range of validity of the simplifications, despite that the assumption $T_p - T_\infty/\widehat{T_s} - T_\infty$ is not always being satisfied. It can be noticed the case of Lienert et al. Al7075 [27], which is quite far from 1. This occurs because the estimation of torque depends on the rotational speed ω, which in the case of this experiment, is too elevated (1,182 r.p.m), whereby the estimated torque is too small, thus generating a wide difference between the values of M and $\widehat{M}$,

It can be noticed that simplification given by Equations (2.2), (2.3), and (2.4) does not influence the result of $M/\widehat{M}$, and despite the slight dependence between Pe and the ratio of torque, the influence of this simplification is not significant enough to be considered in the correction function. This can be corroborated by comparing Cases 1 and 2 from Table (5.2), in which the reduction of the error is infimum, whereby it is considered enough to apply a correction factor that only includes C_1.

It can be observed by comparing Figures (5.10 (a)) and (5.10 (b)), that the correction factor provides a slight improvement to the estimations, since it locates most of them above

the 1:1 trendline, while in the case that does not have the correction factor (Figure (5.10 (a))), the estimations of torque are found mostly above the 1:1 trendline, which indicates that the estimations of torque are higher than the measurement and numerical results, i.e. torque is overpredicted.

In all the figures that plot torque, it can be observed that the experiment from Jain et al. Al2024 [70] remains away from the trendline. This occurs because the prediction of torque is much higher than the experimental value, which happens because, as it was mentioned, the result of $\widehat{M}$ is strongly dependent of the rotational speed ω, which happens to be small enough to generate a higher $\widehat{M}$ value, however, since by observing Figures (5.10 (a)) and (5.10 (b)), it can be noticed that this experiment does not present an excessively high value in comparison to the rest of $\widehat{M}$ data, which indicates that the value of M is relatively small (within the studied range of experiments). An explanation of this behavior lies in possible measurement errors.

In particular, Figure (5.9) illustrates that this experiment, in addition to be away from the 'Y' axis trendline, whose reason is explained previously, is also far from the rest of the data in relation to its position on the 'X' axis. The latter happens because $T_p \ll \widehat{T_s}$, having a particularly small value of T_p, which indicates that the heat supplied by the shoulder due to the friction that this exerts against the base plate is a minimal part of the overall heat that the plate receives during the process.

Related to the sources of error, there exist experimental errors that occur during the experimental trials or test measurements which can lead to altered data. On the other side, there can be originated errors based on assumptions that are not entirely true, for example, Rosenthal's solution [17] assumes constant materials properties, which is not true because some of them change with the variation of temperature, or the case of Zener-Hollomon constants, that for some experiments, were taken from materials with similar properties. There exist as well errors based on mathematical simplifications, such as the case of heat loss through the plate or the process efficiency that where assumed as constant to all of the experiments and they should vary.

Chapter 7

Conclusion

The coupled behavior of heat and plastic deformation involved in the friction stir welding has been validated for an extended set of materials, which involves comparing the published data with the estimations and observing that the model captures the proper trends and orders of magnitude of maximum temperature and torque. In relation to the simplifications imposed on the model, Pe number smaller than one (Equation (2.1)) was always satisfied in both of the cases analyzed, and even thought a small increasing trend was observed in the case of $M/\widehat{M}$, this one is almost negligible for the orders of magnitude in which the work is being performed. Thus, it can be said that Pe number has no mayor influence on the estimations made. On the other hand, the simplification $\widehat{\delta}/a$ (Equation (2.2)) was not always satisfied. It was observed that the ratio of maximum temperature deviates from the asymptotic regime, this means that this simplification has some influence on the estimation of maximum temperature. Thus, Equation (2.2) was considered to improve the accuracy of the estimations mentioned previously. In the case of $\mathrm{V}/\omega\widehat{\delta}$, both studied ratios remain almost constant despite the simplification is not always satisfied.

There is also considered the incorporation of the fourth criterion corresponding to the relation between the preheat temperature due to the shoulder friction and the maximum temperature at the pin/shear layer interface, by observing its respective relation to the ratios of maximum temperature and torque, it was obtained that both studied ratios remain almost constant although the simplification is not always satisfied.

Additionally, the model was readjusted by adding a correction factor that tunes the estimations, making most of them even closer to the numerical results, noting that the former were already capturing the correct trends and orders of magnitude. The correction function captures the errors produced by the simplifications that restrict problem as well as errors generated by the mathematical simplifications made in the scaling analysis. The correction functions followed the correct trends for both ratios plotted against the simplifications.

Finally, it is worth mentioning how crucial is friction stir welding in a variety of industries

such as aerospace engineering and other latest-generation manufacturing industries, whereby there is the imperative need of a formulation of a model that provides relatively simple and accurate approximations whose validity could be tested for different alloys, thus constituting a fundamental advance in the welding field, whose knowledge has been unraveled mostly based on trial and error.

Chapter 8

Future work

Although the model manages to provide a set of formulas that predict satisfactorily the maximum temperature and torque in the welding process, it can be further iterated to achieve even more accurate estimations of the these values. With this in mind, the following recommendations are made:

- Realization of more experiments where the temperature and torque are measured.
- Implement a correction function that more successfully captures the influence of the $\widehat{\delta}/a$ parameter on the estimations.

Bibliography

[1] P. Mendez, K. Tello, and T. Lienert,"*Scaling of coupled heat transfer and plastic deformation around the pin in friction stir welding*", Acta Materialia, vol. 58, no. 18, pp. 6012–6026, 2010.

[2] S. Salazar, "*Coupled model of heat transfer and plastic deformation for friction stir welding (FSW)*", Undergraduate thesis, Universidad de Chile, 2022.

[3] B. Vergara, "*Modelamiento acomplado termico y de deformacion en soldadura por friccion-agitacion*", Master's thesis, Universidad de Chile, 2017.

[4] Y.J. Chao, X. Qi, W. Tang, "*Heat Transfer in Friction Stir Welding – Experimental and Numerical Studies*", Journal of Manufacturing Science and Engineering Transactions of the ASME 125, 138-145, 2003.

[5] P.A. Colgrove, H.R. Shercliff "*Development of Trivex Friction Stir Welding Tool Part 1 – Two Dimensional Flow Modelling and Experimental Validation*", Science and Technology of Welding and Joining 9, 345-351, 2004

[6] A.P. Reynolds, W. Tang, Z. Khandkar, J.A. Khan, K. Linder "*Relationship between weld parameters, hardness distribution and temperature history in alloy 7050 Friction Stir Welding*", Science and Technology of Welding and Joining Vol No 2 190 10, 190-199, 2005. .

[7] H. Schmidt, J. Hattel and J. Wert,"*An analytical model for the heat generation in friction stir welding*"Modelling and Simulation in materials Science and Engineering, 12:143-157, 2003

[8] H.N.B. Schmidt , T.L. Dickerson, J.H. Hattel, "*Material Flow in butt friction stir welds in AA2024-T3*". Acta Materialia, 54(4):1199-1209, 2006.

[9] P. Ulysse, "*Three-dimensional modeling of the friction stir-welding process. International Journal of Machine Tools and Manufacture*",International Journal of Machine Tools and Manufacture, 42(14):1549-1557, 2002.

[10] T. U. Seidel and A. P. Reynolds. "*Two-dimensional friction stir welding process model based on fluid mechanics*", Science And Technology Of Welding And Joining, 8(3):175–183, 2003. 1362-1718.

[11] P.A. Colgrove and H.R. Shercliff, "*Development of a Trivex FSW tool Part 2 - 3D flow modeling*". Science and Technology of Welding and Joining, 9(4):352-361, 2004.

[12] S. Xu, X. Deng, A. P. Reynolds, and T. U. Seidel. "*Finite element simulation of material flow in friction stir welding*", Science And Technology Of Welding And Joining, 6(3):191–193, 2001. 1362-1718.

[13] J. C. McClure, W. Tang, L. E. Murr, X. Guo, Z. Feng, and J. E. Gould. " *A thermal model of friction stir welding*", In Trends in Welding Research, pages 590–595, Pine Mountain, GA, 1998.

[14] Khandkar, M. Z. H., Khan, J. A., and Reynolds, A. P., "*Prediction of temperature distribution and thermal history during friction stir welding: Input torque based model*", Science and Technology of Welding and Joining, 8(3):165-174, 2003. 1362-1718.

[15] C.M. Chen, R. Kovacevic, "*Finite element modeling of friction stir welding—thermal and thermomechanical analysis*Ïnternational Journal of Machine Tools and Manufacture, 43:1319-1326, 2003.

[16] H. Schmidt J. Hattel , "*Modelling heat flow around tool probe in friction stir welding*". Science and Technology of Welding and Joining, 10(2):176-186, 2005.

[17] D. Rosenthal. "*The theory of moving sources of heat and its application to metal treatments*", Transactions of the A.S.M.E., pages 849–866, 1946.
Science And Technology Of Welding And Joining, 10(2):176–186, 2005.

[18] J. A. Dantzig and C. L. Tucker III."*Modeling in Materials Processing*", Cambridge University Press, 2001

[19] W. B. Krantz. "*Scaling Analysis in Modeling Transport and Reaction Processes. A Systematic Approach to Model Building and the Art of Approximation*", John Wiley Sons, INC., 2007.

[20] P. F Mendez."*Advanced scaling techniques for the modeling of materials processing*Ïn Florian Komgoli and Romana G. Reddy, editors, Sohn International Symposium Advanced Processing of Metals and Materials, volume 7, pages 393–404. TMS, 2006.

[21] Ø. Grong. "*Metallurgical Modelling of Welding-First Edition. Institute of Materials*", London, 1994.

[22] K. E.Tello,"*Coupled Model Of Heat Transfer and Plastic Deformation for Friction Stir Welding Using Scaling Analysis*", Master thesis, Colorado School of Mines, 2009.

[23] A. Simar, J. Lecomte-Beckers, T. Pardoen B. de Meester. "*Effect of boundary conditions and heat source distribution on temperature distribution in friction stir welding*", Science and Technology of Welding and Joining, 2006

[24] J. H. Cho, D. E. Boyce, and P. R. Dawson. "*Modeling strain hardening and texture evolution in friction stir welding of stainless steel*". Materials Science And Engineering A-Structural Materials Properties Microstructure And Processing, 398(1-2):146–163, 2005. 0921-5093.

[25] R. Nandan, G. G. Roy, T. J. Lienert, and T. DebRoy. "*Numerical modelling of 3D plastic*

flow and heat transfer during friction stir welding of stainless steel"Science And Technology Of Welding And Joining, 11(5):526–537, 2006. 1362-1718.

[26] "*ASM Handbook Volume 02: Properties and Selection: Nonferrous Alloys and Special-Purpose Materials*", ASM International, 10th edition, 1990.

[27] T.J. Lienert, W.L. Stellwag and H. Shao , "*Determination of Load, Torque, and Tool Temperatures During FSW of Aluminum Alloys*", 2000.

[28] X. K. Zhu and Y. J. Chao. "*Numerical simulation of transient temperature and residual stresses in friction stir welding of 304L stainless steel*". Journal Of Materials Processing Technology, 146(2):263–272, 2004. 0924-0136.

[29] T. J. Lienert, Jr. W. L. Stell, B. B. Grimmett, and R. W. Warke. "*Friction stir welding studies on mild steel*". Welding Journal, pages 1–9, January 2003.

[30] K Ogawa, H Yamaguchi, H Ochi, T Sawai, Y Suga Y Oki, "*Friction welding of AZ31 magnesium alloy, Welding International*", 17:11, 879-885, 2003.

[31] Tremblay, D.A., Bouchard, D., Kiss, L., "*Dynamic wetting spread factors and interfacial heat transfer coefficients in the solidification of aluminum droplets on copper substrates*". Canada National Research Concuil Publications Archive, 2005.

[32] International Standard Organization, "*Wrought aluminium and aluminium alloys — Sheets, strips and plates — Part 2: Mechanical properties*", ISO 6361-2, 3rd Edition, pp 6, ISO 6361-2:2011(E), 2011.

[33] Chen, J.K., Hung, H., Wang, C., Tang, N., "*Thermal and electrical conductivity in Al–Si/Cu/Fe/Mg binary and ternary Al alloys*", Journal of Materials Science, 50, 50:5630–5639, 2015.

[34] Anastasios D. Kostrivas and John C. Lippold. "*Simulating weld-fusion boundary microstructures in aluminum alloys*". JOM Journal of the Minerals, Metals and Materials Society, 56(2):65–72, 2004.

[35] K. Hemantha Vepakomma, Peter N. Kalu, and N. Chandra. "*Three dimensional thermal modeling of friction stir processing*". Master thesis, The Florida State University, 2006.

[36] Srinivasarao B., Lefebvre, W., "*Effect of cryorolling on the microstructure and mechanical properties of AA2198 alloy*", Proceedings of the 12th International Conference on Aluminium Alloys, pp. 1961-1965, 2010.

[37] Gazizov, M., Teleshov, V., Zakharov, V., Kaibyshev, R., "*Solidification behaviour and the effects of homogenisation on the structure of an Al–Cu–Mg–Ag–Sc alloy*", Journal of Alloys and Compounds, Volume 509, Issue 39, pp. 9497-9507, ISSN 0925-8388, 2011.

[38] Sutton, M.A., Reynolds, A.P., Yan, J., Yang, B., Yuan, N., "*Microstructure and mixed mode I/II fracture of AA2524-T351 base material and friction stir welds*", Engineering Fracture Mechanics, Volume 73, Issue 4, pp. 391-407, ISSN 0013-7944, 2006.

[39] Xiong, J., Peng, X., Shi, J., Wang, Y., Sun, J., Liu, X., Li, J., "*Numerical simulation*

of thermal cycle and void closing during friction stir spot welding of AA-2524 at different rotational speeds", Materials Characterization, Volume 174, 110984, ISSN 1044-5803, 2021.

[40] J. Tsui,"*Experimental studies and asymptotic scaling for the development of engineering tools to predict coupled heat transfer and plastic deformation in Friction Stir Welding (FSW)*", Master's thesis, University of Alberta, 2016.

[41] Silva, A., De Backer, J., Bolmsjö, G., "*Temperature measurements during friction stir welding*". The International Journal of Advanced Manufacturing Technology. 88:2899–2908, 2017.

[42] El-Shennawy, M., Abdel-Aziz, K., Omar, A., "*Metallurgical and Mechanical Properties of Heat Treatable Aluminum Alloy AA6082 Welds*". International Journal of Applied Engineering Research. 12(11);2832-2839, 2017.

[43] Hovanski, Y., Mishra, R., Sato, Y., Upadhyay, P., Yan, D. (eds) "*Friction Stir Welding and Processing X. The Minerals, Metals Materials Series*", Springer, Cham, 9th Edition, pp 91–98, 2019.

[44] Kim, K., Lim, Y., Shin, J., Ko, S., Kim, J., "*Effects of Zn and Mg Amounts on the Properties of High Thermal Conductivity Al-Zn-Mg-Fe Alloys for Die Casting*", Journal of the Korea Foundry Society, 33, 113-121, 2013.

[45] Muhsin J. J., Moneer H., Tolephih and Muhammed A. M., "*Numerical and experimental analysis of transient temperature and residual thermal stresses in friction stir welding of aluminum alloy 7020-T53*". Journal of Engineering, Vol 18, No6, 11. 11663-11674, 2012.

[46] Hamilton, C., Dymek, S., Kalemba I., Blicharski M., "*Friction stir welding of aluminium 7136-T76511 extrusions*", Science and Technology of Welding and Joining, 13:8, 714-720, 2008.

[47] Wong, W. A., Bucci, R. J., Stentz, R. H., Conway, J. B., "*Tensile and Strain-Controlled Fatigue Data for Certain Aluminum Alloys for Application in the Transportation Industry*", SAE Transactions Vol. 96, Section 1, pp. 373-383, 1987.

[48] Haitao Zhang, Hiromi Nagaumi, Yubo Zuo, Jianzhong Cui, "*Coupled modeling of electromagnetic field, fluid flow, heat transfer and solidification during low frequency electromagnetic casting of 7XXX aluminum alloys: Part 1: Development of a mathematical model and comparison with experimental results*", Materials Science and Engineering: A, Volume 448, Issues 1–2, pp. 189-203, ISSN 0921-5093, 2007.

[49] Li, S., Yang, S., Lu, Q. et al. "*A Novel Shim-Assisted Resistance Spot Welding Process to Improve Weldability of Medium-Mn Transformation-Induced Plasticity Steel*". Metall Mater Trans B 50, 1–9, 2019.

[50] Sarkar, B., Deva, A., S.MukhopadhyayB.K.Jha, Mukerjee, D., Mathur, A.S., "*Processing and application of interstitial free(IF) grade steel: Prospects in SAIL*", International Conference on Interstitial Free Steels: Manufacturing and Applications IFSTEEL, 2010.

[51] Askeland, D.R., Fulay, P.P., Wright W.J., "*The Science and Engineering of Materials*", CENGAGE Learning, 6th Edición, pp. 495, 2016.

[52] "*Metals Handbook Desk Edition*", ASM International, 2nd Edition, pp. 153-173, 1998.

[53] A.A Howe. "*Estimation of liquidus temperatures for steels*". Ironmaking and Steelmaking, 15(3):134–142, 1988.

[54] Jyrki Miettinen. "*Calculation of solidification-related thermophysical properties for steel*". Metallurgical and Materials Transactions B, 28B:281–297, 1197.

[55] Hamilton, C., Dymek, S., Sommers, A., "*Characteristic temperature curves for aluminum alloys during friction stir welding*". Welding Journal (Miami, Fla). 89, 189s-194s, 2010.

[56] Senkova, S., Senkov, O., Miracle, D., "*Cryogenic and elevated temperature strengths of an Al-Zn-Mg-Cu alloy modified with Sc and Zr*". Metallurgical and Materials Transactions A. 37. 3569-3575. 2006.

[57] Song, Y., Perez, C., Esteves, G., Lundh, J., Saltonstall, C., Beechem, T., Yang, J., Ferri, K., Brown, J., Tang, Z., Maria, J.P., Snyder, D., Olsson, R., Griffin, B., Trolier-McKinstry, S., Foley, B., Choi, S., "*Thermal Conductivity of Aluminum Scandium Nitride for 5G Mobile Applications and Beyond*". ACS applied materials interfaces, 13(16), 2021.

[58] Jiang, B., Liu, W., Chen, S., Yang, Q., Pan, F., "*Mechanical properties and microstructure of as-extruded AZ31 Mg alloy at high temperatures*", Materials Science and Engineering: A, 530, pp. 51-56, ISSN 0921-5093, 2011.

[59] Han, T., Huang, G., Li, H., Wang, L., Zhang, H., Pan, F., "*Strength-ductility balance of AZ31 magnesium alloy via accumulated extrusion bonding combined with two-stage artificial cooling*", Journal of Magnesium and Alloys, ISSN 2213-9567, 2021.

[60] Li, S., Yang, X., Hou, J., Du, W., "*A review on thermal conductivity of magnesium and its alloys, Journal of Magnesium and Alloys*", Volume 8, Issue 1, pp 78-90, ISSN 2213-9567, 2020.

[61] Le, V.T., Goo, N.S. Kim, J.Y. "*Experimental investigation on thermal contact resistance of alumina fibrous insulation material with Ti-6Al-4V alloy at high temperature and its effective thermal conductivity*", Heat Mass Transfer 55, 1705–1721, 2019.

[62] C. Sellars and W. M. Tegart, "*Hot workability*", International Metallurgical Reviews, p. 17:1–23, 1972.

[63] K. E. Tello, A. P. Gerlich and P. F. Mendez, "*Constants for hot deformation constitutive models for recent experimental data*", Science and Technology of Welding Joining 15(3), 2010.

[64] Bombač, D., Cvahte, P., Balog, M., Kugler, G., Terčelj, M., "*In-Depth Comparison of an Industrially Extruded Powder and Ingot Al Alloys*". Metals - Open Access Metallurgy Journal. 11, 1484, 2020.

[65] He, H.., Yi, Y., Cui, J., Huang, S., "*Hot deformation characteristics and processing*

parameter optimization of 2219 Al alloy using constitutive equation and processing map". Vacuum. 160. 293–302, 2018.

[66] Gupta, R.K., Anil Kumar V., Krishnan, A., Niteshraj, J., "*Hot Deformation Behavior of Aluminum Alloys AA7010 and AA7075. Journal of Materials Engineering and Performance*". 28. 1059-9495, 2019.

[67] Ghosh, S., Somani, M.C., Setman, D., Mula, S., "*Hot Deformation Characteristic and Strain Dependent Constitutive Flow Stress Modelling of Ti+Nb Stabilized Interstitial Free Steel*". Met. Mater. Int. 27, 2481–2498, 2021.

[68] Sheikhani, A., Roumina, R., Mahmudi, R., "*Hot deformation behavior of an extruded AZ31 alloy doped with rare-earth elements*", Journal of Alloys and Compounds, Volume 852, 156961, ISSN 0925-8388, 2021.

[69] S Benavides, Y Li, L.E Murr, D Brown, J.C McClure, "*Low-temperature friction-stir welding of 2024 aluminum*", Scripta Materialia, Volume 41, Issue 8, pp. 809-815, ISSN 1359-6462, 1999.

[70] Jain, R., Pal, S., Singh, S., "*A study on the variation of forces and temperature in a friction stir welding process: A finite element approach*". Journal of Manufacturing Processes. 23. 278-286, 2016.

[71] P.A. Colgrove and H.R. Shercliff, "*Experimetal and Numerical analysis of Al 7075-T7351 FSW*". Science and Technology of Welding and Joining, 8(5):360-368, 2003.

[72] T. J. Lienert. "*Microstructures and Mechanical Properties of Friction Stir Welds in Titanium Alloys*". In R. Mishra and M. Mahoney, editors, Friction Stir Welding and Processing, chapter 7, pages 123–154. ASM International, 2007.

[73] Vardanjani, M.J., Araee, A., Senkara, J., Jakubowski, J., Godek, J. "*Experimental and numerical analysis of shunting effect in resistance spot welding of Al2219 sheets*". Bulletin of The Polish Academy of Sciences-technical Sciences, 64, 425-434, 2016.

[74] Nie, L. Wu, Y. Gong, H. "*Prediction of temperature and residual stress distributions in friction stir welding of aluminum alloy*". The International Journal of Advanced Manufacturing Technology, 106:3301–3310, 2020.

[75] Ding, X., Zhao, F., Shuang, Y., Ma, L., Chu, Z., Zhao, C., "*Characterization of hot deformation behavior of as-extruded AZ31 alloy through kinetic analysis and processing maps*", Journal of Materials Processing Technology, Volume 276, 116325, ISSN 0924-0136, 2020

[76] R.W. Fondaa and J.F. Bingert, "*Texture variations in an aluminum friction stir weld*", Scripta Materialia, 57(11):1052-1055,2007.

[77] Judy Schneider, Ronald Beshears, Arthur C. Nunes Jr., "*Interfacial sticking and slipping in the friction stir welding process*", Materials Science and Engineering A, 435-436:297-304, 2006.

[78] Yuh J. Chao, X. Qi and W. Tang, "*Heat Transfer in Friction Stir Welding — Experimental and Numerical Studies*", Journal of Manufacturing Science and Engineering, 125(1):8, 2003.

[79] Kevin J. Colligan, "*Relationships between process variables related to heat generation in friction stir welding of aluminum*", Friction Stir Welding Processing IV, 4:39-54, 2007.

[80] Z.W. Chen, T. Pasang, Y. Qi, "*Shear flow and formation of Nugget zone during friction stir welding of aluminum alloy 5083-O*". Materials Science and Engineering A,474(1-2):312-316, 2008.

[81] T. Long, W. Tang and A. P. Reynolds, "*Process response parameter relationships in aluminium alloy friction stir welds*", Sciece and Technology of Welding and Joining, 12(4):311-317, 2007.

[82] G.G. Roy, R. Nandan, T. DebRoy, "*Dimensionless Correlation to estimate Peak Temperature During FSW*", Science and Technology of Welding and Joining, 11:606-608, 2006.

[83] R. Nandan, G.G. Roy, T. DebRoy , "*Numerical simulation of 3D Heat Transfer and Plastic Flow During friction stir Welding*", Metallurgical and Materials Transactions A, 37A(4):1247-1259, 2006.

[84] M. Song and R. Kovacevic, "*Thermal Modeling of FSW in a moving coordinate system and its validation*", International Journal of Machine Tool and Manufacture, 43:605-615, 2003.

[85] M. Guerra, C. Schmidt, J.C. McClure, L.E. Murr, A.C. Nunes, "*Flow patterns during friction stir welding*". Materials Characterization, 49:95-101, 2003.

[86] Shaowen Xu and Xiaomin Deng, "*A study of texture patterns in friction stir welds*", Acta Materialia, 2008.

[87] H. Atharifar, D. C. Lin, and R. Kovacevic , "*Studying Tunnel-like Defect in Friction Stir Welding Process Using Computational Fluid Dynamics*". Numerical, Mathematical, and Physical Modelling Tools for Materials Processes II, pages 375-391, 2007.

[88] Wanchuck Woo, Levente Balogh, Tamás Ungár, Hahn Choo, Zhili Feng, "*Grain structure and dislocation density measurements in a friction-stir welded aluminum alloy using X-ray peak profile analysis*", Materials Science and Engineering A, 498(1-2):308-313, 2008.

[89] Assidi, Mohamed, Fourment, Lionel, Guerdoux, Simon, Nelson, Tracy, "*Friction models for friction stir welding process simulation: calibrations from welding experiments*", International Journal of Machine Tools and anufacture, 50(2):143-155, 2010.

[90] A.P. Reynolds, Z. Khandkar, T. Long, W. Tang and J. Khan, "*Utility of relatively simple models for understanding process parameter effects of FSW*". Thermec'2003, 426-4(1):2959-2964, 2003.

[91] G. Buffa, L. Fratini, R. Shivpuri, "*CDRX modelling in friction stir welding of AA7075-T6 aluminum alloy: Analytical approaches*", Journal of Mteroals Processing Technology,

191(1-3):356-359, 2007.

[92] T.J. Lienert, W.L. Stellwag, Jr. and L.R. Lehman, "*Process Results for FSW of Ti-6Al-4V*". Welding Journal, pages 1-9, January 2003.

[93] Bangcheng Yang, Junhui Yan, Michael A. Sutton, Anthony P. Reynolds, "*Banded microstructure in AA2024-T351 and AA2524-T351 aluminum friction stir welds*". Materials Science and Engineering A364, 364:55-65, 2004.

[94] H. Schmidt and J. Hattel, "*A local model for the thermomechanical conditions in friction stir welding*". Modelling and Simulation In Materials Science and Engineering. 13(1):77-93, 2005.

[95] Dongun Kim, Harsha Badarinarayan, Ji Hoon Kim, Chongmin Kim, Kazutaka Okamoto, R.H. Wagoner, Kwansoo Chung, "*Numerical simulation of friction stir butt welding process for AA5083-H18 sheets*". European Journal of Machine, A/solids, 29(2):204-2015. 2010.

[96] R. Nandan, G.G. Roy, T.J. Lienert, T. Debroy , "*Three-dimensional heat and material flow during friction stir welding of mild steel*". Acta Materialia, 55(3):883-895, 2007.

[97] J, Adamowski Szkodo, Marek. "*Friction Stir Welds (FSW) of aluminium alloy AW6082-T6*". Journal of Achievements in Materials and Manufacturing Engineering. Vol 20. Issues 1-2, 2007.

[98] Ho-Sung Lee, Jong-Hoon Yoon, Joon-Tae Yoo, Kookil No, "*Friction Stir Welding Process of Aluminum-lithium Alloy 2195*", Procedia Engineering, Volume 149, pp. 62-66, ISSN 1877-7058, 2016.

[99] Tang, W., Guo, X., Mcclure, J., Murr, L., Nunes, A.C., "*Heat Input and Temperature Distribution in Friction Stir Welding*". Journal of Materials Processing Manufacturing Science - J MATER PROCESS MANUF SCI. 7. 163-172, 1998.

[100] Boz, Mustafa Kurt, Adem. "*The Influence of Stirrer Geometry on Bonding and Mechanical Properties in Friction Stir Welding Process*". Materials Design. 25. 343-347, 2004.

[101] Muhsin, J., Moneer T., Muhammed, S., "*Effect of friction stir welding parameters (rotation and transverse) speed on the transient temperature distribution in friction stir welding of AA 7020-t53*". ARPN Journal of Engineering and Applied Sciences. 7. 436-446. 2012

[102] Verma, S., Gupta, M., Misra, P. "*Study on temperature distribution during Friction Stir Welding of 6082 aluminum alloy*". 5th International Conference of Materials Processing and Characterization, Materials Today: Proceedings 4 (2017) 1350–1356, 2016.

[103] M. Sadoun, A. Wagih, A. Fathy, A.R.S. Essa, "*Effect of tool pin side area ratio on temperature distribution in friction stir welding*", Results in Physics, Volume 15, 102814, ISSN 2211-3797, 2019.

[104] Edwards, P., Ramulu M., "*Peak temperatures during friction stir welding of Ti–6Al–4V*", Science and Technology of Welding Joining, Vol. 15, Issue 6, pp. 468-472, 2010.

[105] C. Hamilton, A. Sommers, S. Dymek, "*A thermal model of friction stir welding applied*

to Sc-modified Al–Zn–Mg–Cu alloy extrusions", International Journal of Machine Tools and Manufacture, Volume 49, Issues 3–4, pp. 230-238, ISSN 0890-6955, 2009.

[106] Rui-dong Fu, Jian-feng Zhang, Yi-jun Li, Ju Kang, Hui-jie Liu, Fu-cheng Zhang, "*Effect of welding heat input and post-welding natural aging on hardness of stir zone for friction stir-welded 2024-T3 aluminum alloy thin-sheet*", Materials Science and Engineering: A, Volume 559, pp. 319-324, ISSN 0921-5093, 2013.

[107] Genevois C., Fabrègue, D., Deschamps, A., Poole, W.J., "*On the coupling between precipitation and plastic deformation in relation with friction stir welding of AA2024 T3 aluminium alloy*", Materials Science and Engineering: A, Volume 441, Issues 1–2, pp. 39-48, ISSN 0921-5093, 2006.

[108] Mohammadtaheri, M., Haddad-Sabzevar, M., Mazinani, M. et al. "*The Effect of Base Metal Conditions on the Final Microstructure and Hardness of 2024 Aluminum Alloy Friction-Stir Welds*". Metall Mater Trans B 44, 738–743, 2013.

[109] M. Jariyaboon, A.J. Davenport, R. Ambat, B.J. Connolly, S.W. Williams, D.A. Price, "*The effect of welding parameters on the corrosion behaviour of friction stir welded AA2024–T351*", Corrosion Science, Volume 49, Issue 2, pp. 877-909, ISSN 0010-938X, 2007.

[110] F.F. Wang, W.Y. Li, J. Shen, S.Y. Hu, J.F. dos Santos, "*Effect of tool rotational speed on the microstructure and mechanical properties of bobbin tool friction stir welding of Al–Li alloy*", Materials Design, Volume 86, pp. 933-940, ISSN 0264-1275, 2015.

[111] Upadhyay, P. Reynolds, A.P., "*Effects of thermal boundary conditions in friction stir welded AA7050-T7 sheets*". Materials Science and Engineering: A. 527. 1537-1543. 2010.

[112] Fu Rui-dong, Sun Zeng-qiang, Sun Rui-cheng, Li Ying, Liu Hui-jie, Liu Lei, "*Improvement of weld temperature distribution and mechanical properties of 7050 aluminum alloy butt joints by submerged friction stir welding*", Materials Design, Volume 32, Issue 10, pp. 4825-4831, ISSN 0261-3069, 2011.

[113] Kh. A. A. Hassan, P. B. Prangnell, A. F. Norman, D. A. Price S. W. Williams "*Effect of welding parameters on nugget zone microstructure and properties in high strength aluminium alloy friction stir welds*", Science and Technology of Welding and Joining, 8:4, 257-268, ISSN: 1362-1718. 2003.

[114] S. Lu, D.L. Yang, S.Y. Xiao, S.J. Chen, "*Three-dimensional investigation on temperature distribution and mechanical properties of AZ31Mg alloy joint welded by FSW*", Proceedings of the 1st International Joint Symposium on Joining and Welding, Woodhead Publishing, pp. 67-72, ISBN 9781782421634, 2013.

[115] H. Fujii, L. Cui, N. Tsuji, M. Maeda, K. Nakata, K. Nogi, "*Friction stir welding of carbon steels*", Materials Science and Engineering A 429, 50–57, 2006.

[116] Y.C. Chen, J.C. Feng, H.J. Liu, "*Precipitate evolution in friction stir welding of 2219-T6 aluminum alloys*", Materials Characterization, Volume 60, Issue 6, pp. 476-481, ISSN

1044-5803, 2009.

[117] Weifeng Xu, Jinhe Liu, Guohong Luan, Chunlin Dong, "*Temperature evolution, microstructure and mechanical properties of friction stir welded thick 2219-O aluminum alloy joints*", Materials Design, Volume 30, Issue 6, pp. 1886-1893, ISSN 0261-3069, 2009.

[118] Zhang, H. Liu, Huijie Yu, Lanfang. "*Effect of Water Cooling on the Performances of Friction Stir Welding Heat-Affected Zone. Journal of Materials Engineering and Performance*". 21(7), 2011.

[119] Z. Zhang, B.L. Xiao, Z.Y. Ma, "*Hardness recovery mechanism in the heat-affected zone during long-term natural aging and its influence on the mechanical properties and fracture behavior of friction stir welded 2024Al–T351 joints*", Acta Materialia 73, 227–239, 2014.

[120] Harpreet Sidhar, Rajiv S. Mishra, "*Aging kinetics of friction stir welded Al-Cu-Li-Mg-Ag and Al-Cu-Li-Mg alloys*", Materials Design, Volume 110, pp. 60-71, ISSN 0264-1275, 2016.

Annexes

Annex A. Summary of temperature data compiled from literature

Table A.1: Maximum temperature from the literature and estimation of maximum temperature for each experiment part 1.

Author	Material	Especification	T_s [°K]	$\widehat{T_s}$[°K]
H. Schmidt	Aluminum	AA2024	673.0	747.0
Yuh J. Chao	Aluminum	AA2195	698.0	918.7
Yuh J. Chao	Aluminum	AA2195	678.0	913.8
K. J. Colligan	Aluminum	AA5083	803.0	1020.9
K. J. Colligan	Aluminum	AA5083	818.0	1004.1
K. J. Colligan	Aluminum	AA5083	848.0	986.4
T.J. Lienert	Aluminum	AA5083	623.0	860.6
M. Z. H. Khandkar	Aluminum	AA6061	683.0	825.1
G.G. Roy	Aluminum	AA6061	820.0	895.5
G.G. Roy	Aluminum	AA6061	770.0	845.3
G.G. Roy	Aluminum	AA6061	773.0	832.7
G.G. Roy	Aluminum	AA6061	766.0	828.1
G.G. Roy	Aluminum	AA6061	755.0	831.5
G.G. Roy	Aluminum	AA6061	742.0	823.7
G.G. Roy	Aluminum	AA6061	736.0	823.7
G.G. Roy	Aluminum	AA6061	729.0	823.7
G.G. Roy	Aluminum	AA6061	791.0	833.0
G.G. Roy	Aluminum	AA6061	795.0	833.2
G.G. Roy	Aluminum	AA6061	799.0	833.4
G.G. Roy	Aluminum	AA6061	820.0	881.7
G.G. Roy	Aluminum	AA6061	818.0	880.9
G.G. Roy	Aluminum	AA6061	814.0	879.6

Table A.2: Maximum temperature from the literature and estimation of maximum temperature for each experiment part 2.

Author	Material	Especification	T_s [°K]	$\widehat{T_s}$[°K]
R. Nandan	Aluminum	AA6061	790.0	879.3
R. Nandan	Aluminum	AA6061	745.0	824.4
R. Nandan	Aluminum	AA6061	685.0	823.4
R. Nandan	Aluminum	AA6061	790.0	828.3
R. Nandan	Aluminum	AA6061	700.2	823.7
R. Nandan	Aluminum	AA6061	694.4	823.7
R. Nandan	Aluminum	AA6061	688.2	823.7
R. Nandan	Aluminum	AA6061	762.7	833.4
R. Nandan	Aluminum	AA6061	756.0	833.2
R. Nandan	Aluminum	AA6061	749.6	833.0
R. Nandan	Aluminum	AA6061	807.4	881.7
R. Nandan	Aluminum	AA6061	801.5	880.9
R. Nandan	Aluminum	AA6061	797.3	879.6
M. Z. H. Khandkar	Aluminum	AA6061	665.0	825.1
T.J. Lienert	Aluminum	AA6061	625.0	830.5
M. Assidi	Aluminum	AA6061	820.0	829.3
M. Assidi	Aluminum	AA6061	768.0	829.3
M. Assidi	Aluminum	AA6061	781.0	829.3
M. Assidi	Aluminum	AA6061	803.0	829.3
A.P. Reynolds.	Aluminum	AA7050	506.0	721.8
A.P. Reynolds.	Aluminum	AA7050	589.0	721.8
A.P. Reynolds.	Aluminum	AA7050	638.0	721.8
A.P. Reynolds.	Aluminum	AA7050	663.0	722.0
A.P Reynolds.	Aluminum	AA7050	592.0	721.8
A.P Reynolds.	Aluminum	AA7050	671.0	721.9
A.P Reynolds.	Aluminum	AA7050	661.0	724.9
A.P Reynolds.	Aluminum	AA7050	703.0	772.7
P.A. Colgrove	Aluminum	AA7075	803.0	1459.7
P.A. Colgrove	Aluminum	AA7075	813.0	1284.9
P.A. Colgrove	Aluminum	AA7075	823.0	1133.1
P.A. Colgrove	Aluminum	AA7075	808.0	1002.4
P.A. Colgrove	Aluminum	AA7075	813.0	954.0
P.A. Colgrove	Aluminum	AA7075	803.0	910.9
P.A. Colgrove	Aluminum	AA7075	798.0	872.3
P.A. Colgrove	Aluminum	AA7075	803.0	826.0
P.A. Colgrove	Aluminum	AA7075	808.0	812.5
P.A. Colgrove	Aluminum	AA7075	798.0	800.8
P.A. Colgrove	Aluminum	AA7075	773.0	833.1

Table A.3: Maximum temperature from the literature and estimation of maximum temperature for each experiment part 3.

Author	Material	Especification	T_s [°K]	$\widehat{T_s}$[°K]
P.A. Colgrove	Aluminum	AA7075	793.0	805.4
P.A. Colgrove	Aluminum	AA7075	758.0	794.5
P.A. Colgrove	Aluminum	AA7075	738.0	785.3
P.A. Colgrove	Aluminum	AA7075	773.0	763.8
T.J. Lienert	Aluminum	AA7075	604.0	901.1
R. Nandan	Steel	304SS	570.0	1622.2
X.K. Zhu and Y.J. Chao	Steel	304SS	1243.0	1622.4
G.G. Roy	Steel	304SS	1430.0	1620.4
G.G. Roy	Steel	304SS	1412.0	1620.8
G.G. Roy	Steel	304SS	1518.0	1621.5
G.G. Roy	Steel	304SS	1316.0	1620.5
G.G. Roy	Steel	304SS	1313.0	1620.7
G.G. Roy	Steel	304SS	1385.0	1621.2
G.G. Roy	Steel	304SS	1241.0	1620.4
G.G. Roy	Steel	304SS	1200.0	1620.4
G.G. Roy	Steel	304SS	1256.0	1620.6
G.G. Roy	Steel	304SS	1314.0	1620.9
G.G. Roy	Steel	SAE1018	1428.0	1670.8
G.G. Roy	Steel	SAE1018	1506.0	1674.5
G.G. Roy	Steel	SAE1018	1349.0	1668.3
G.G. Roy	Steel	SAE1018	1286.0	1668.1
G.G. Roy	Steel	SAE1018	1236.0	1667.8
G.G. Roy	Steel	SAE1018	1359.0	1670.3
G.G. Roy	Steel	SAE1018	1301.0	1669.8
G.G. Roy	Steel	SAE1018	1423.0	1673.8
G.G. Roy	Steel	SAE1018	1361.0	1672.7
G.G. Roy	Steel	SAE1018	1273.0	1668.3
T.J. Lienert	Steel	SAE1018	938.0	1665.8
T.J. Lienert	Titanium	Ti-6Al-4V	1143.0	1711.1
B. Yang	Aluminum	AA2024	788.0	747.3
B. Yang	Aluminum	AA2024	763.0	747.3
B. Yang	Aluminum	AA2024	603.0	747.0
C.M. Chen and R. Kovacevic	Aluminum	AA6061	653.0	823.5
C.M. Chen and R. Kovacevic	Aluminum	AA6061	764.0	823.4
H. Schmidt and J. Hattel	Aluminum	AA2024	773.0	747.0
H. Schmidt & J. Hattel	Aluminum	AA2024	708.0	747.0
D. Kim	Aluminum	AA5083	798.0	812.5
D. Kim	Aluminum	AA5083	798.0	812.5

Table A.4: Maximum temperature from the literature and estimation of maximum temperature for each experiment part 4.

Author	Material	Especification	T_s [°K]	$\widehat{T_s}$[°K]
D. Kim	Aluminum	AA5083	733.0	812.4
D. Kim	Aluminum	AA5083	740.0	812.4
D. Kim	Aluminum	AA5083	803.0	823.7
D. Kim	Aluminum	AA5083	813.0	823.7
R. Nandan	Steel	SAE1018	1463.0	1668.3
R. Nandan	Steel	SAE1018	1170.0	1666.9
R. Nandan	Steel	SAE1018	1137.6	1666.9
R. Nandan	Steel	SAE1018	1106.9	1666.9
R. Nandan	Steel	SAE1018	1061.0	1666.9
R. Nandan	Steel	SAE1018	1229.2	1668.4
R. Nandan	Steel	SAE1018	1168.0	1668.4
R. Nandan	Steel	SAE1018	1140.1	1668.4
R. Nandan	Steel	SAE1018	1097.2	1668.4
R. Nandan	Steel	SAE1018	1292.7	1670.9
R. Nandan	Steel	SAE1018	1210.5	1670.9
R. Nandan	Steel	SAE1018	1170.0	1670.9
R. Nandan	Steel	SAE1018	1128.3	1670.9
R. Nandan	Steel	SAE1018	1350.6	1674.8
R. Nandan	Steel	SAE1018	1253.9	1674.8
R. Nandan	Steel	SAE1018	1193.2	1674.7
R. Nandan	Steel	SAE1018	1152.3	1674.7
J. Adamowski	Aluminum	AA6082	513.0	921.5
Ho-Sung Lee	Aluminum	AA2195	480.0	1980.2
W. Tang	Aluminum	AA6061	698.0	823.3
W. Tang	Aluminum	AA6061	723.0	823.3
W. Tang	Aluminum	AA6061	728.0	824.1
W. Tang	Aluminum	AA6061	748.0	829.0
B. Mustafa	Aluminum	AA1080	610.0	1001.5
R. Jain	Aluminum	AA2024	756.0	878.1
R. Jain	Aluminum	AA2024	818.0	1535.6
R. Jain	Aluminum	AA2024	843.0	3917.6
J. J. Muhsin	Aluminum	AA7020	629.0	921.8
J. J. Muhsin	Aluminum	AA7020	642.0	921.8
J. J. Muhsin	Aluminum	AA7020	615.0	899.2
J. J. Muhsin	Aluminum	AA7020	680.0	922.0
S Verma	Aluminum	AA6082	532.0	821.4
S Verma	Aluminum	AA6082	521.0	821.4
S Verma	Aluminum	AA6082	528.0	821.4

Table A.5: Maximum temperature from the literature and estimation of maximum temperature for each experiment part 5.

Author	Material	Especification	T_s [°K]	$\widehat{T_s}$[°K]
S Verma	Aluminum	AA6082	557.0	821.4
S Verma	Aluminum	AA6082	534.0	821.4
A.M. Sadoun	Aluminum	AA7075	658.0	761.1
A.M. Sadoun	Aluminum	AA7075	638.0	761.1
A.M. Sadoun	Aluminum	AA7075	627.0	761.1
P. Edwards and M. Ramulu	Titanium	Ti-6Al-4V	1277.0	1711.2
P. Edwards and M. Ramulu	Titanium	Ti-6Al-4V	1373.0	1712.8
P. Edwards and M. Ramulu	Titanium	Ti-6Al-4V	1422.0	1716.1
P. Edwards and M. Ramulu	Titanium	Ti-6Al-4V	1385.0	1713.5
P. Edwards and M. Ramulu	Titanium	Ti-6Al-4V	1361.0	1712.0
C. Hamilton	Aluminum	SSA038	619.0	769.6
C. Hamilton	Aluminum	SSA038	623.0	771.5
C. Hamilton	Aluminum	SSA038	645.0	780.4
C. Hamilton	Aluminum	SSA038	663.0	851.3
C. Hamilton	Aluminum	SSA038	586.0	769.6
C. Hamilton	Aluminum	SSA038	593.0	771.5
C. Hamilton	Aluminum	SSA038	638.0	780.4
C. Hamilton	Aluminum	SSA038	664.0	851.3
Rui-dong Fu	Aluminum	AA2024	608.0	747.0
Rui-dong Fu	Aluminum	AA2024	673.0	747.0
Rui-dong Fu	Aluminum	AA2024	708.0	747.0
Rui-dong Fu	Aluminum	AA2024	728.0	747.0
S. Benavides	Aluminum	AA2024	603.0	750.1
S. Benavides	Aluminum	AA2024	413.0	750.1
C. Genevois	Aluminum	AA2024	613.0	754.4
B. Yang	Aluminum	AA2024	598.0	747.0
B. Yang	Aluminum	AA2024	753.0	747.0
B. Yang	Aluminum	AA2024	788.0	747.0
B. Yang	Aluminum	AA2524	578.0	785.0
B. Yang	Aluminum	AA2524	653.0	785.0
B. Yang	Aluminum	AA2524	673.0	785.3
M. Mohammadtaheri	Aluminum	AA2024	725.0	2050.9
M. Mohammadtaheri	Aluminum	AA2024	706.0	2050.9
M. Jariyaboon	Aluminum	AA2024	754.0	748.9
M. Jariyaboon	Aluminum	AA2024	523.0	747.0
M. Jariyaboon	Aluminum	AA2024	548.0	748.8
M. Jariyaboon	Aluminum	AA2024	573.0	747.3
M. Jariyaboon	Aluminum	AA2024	545.0	747.0

Table A.6: Maximum temperature from the literature and estimation of maximum temperature for each experiment part 6.

Author	Material	Especification	T_s [°K]	$\widehat{T_s}$[°K]
M. Jariyaboon	Aluminum	AA2024	603.0	748.9
F.F. Wang	Aluminum	AA2198	525.0	797.8
F.F. Wang	Aluminum	AA2198	540.0	824.6
F.F. Wang	Aluminum	AA2198	575.0	864.5
F.F. Wang	Aluminum	AA2198	603.0	918.4
P. Upadhyay	Aluminum	AA7050	683.0	721.8
P. Upadhyay	Aluminum	AA7050	743.0	742.0
P. Upadhyay	Aluminum	AA7050	773.0	970.0
Rui-dong Fu	Aluminum	AA7050	643.0	732.8
Kh. A. A. Hassan	Aluminum	AA7010	674.0	760.6
Kh. A. A. Hassan	Aluminum	AA7010	749.0	760.7
Kh. A. A. Hassan	Aluminum	AA7010	740.0	760.6
C. Hamilton	Aluminum	AA7136	587.0	736.8
C. Hamilton	Aluminum	AA7136	688.0	789.0
S Lu	Magnesium	AZ31	722.0	861.2
H. Fujii	Steel	IF	916.0	1707.3
H. Fujii	Steel	IF	1112.0	1707.3
H. Fujii	Steel	SAE1012	1063.0	1628.8
H. Fujii	Steel	SAE1012	913.0	1628.8
H. Fujii	Steel	SAE1035	1146.0	1591.8
H. Fujii	Steel	SAE1035	1014.0	1591.8
H. Fujii	Steel	SAE1035	926.0	1591.8
Y.C. Chen	Aluminum	AA2219	740.0	782.3
Weifeng Xu	Aluminum	AA2219	665.0	877.1
Weifeng Xu	Aluminum	AA2219	674.0	936.4
Weifeng Xu	Aluminum	AA2219	666.0	932.2
H.J. Zhang	Aluminum	AA2219	693.0	822.4
H.J. Zhang	Aluminum	AA2219	671.0	822.4
Z. Zhang	Aluminum	AA2024	613.0	767.2
Harpreet	Aluminum	AA2195	783.0	1766.9
Harpreet	Aluminum	AA2199	803.0	1364.0
J. Tsui	Aluminum	AA5059	668.1	816.5
J. Tsui	Aluminum	AA5059	718.2	817.3
J. Tsui	Aluminum	AA5059	761.6	830.0
J. Tsui	Aluminum	AA5059	708.1	817.3
J. Tsui	Aluminum	AA5059	760.9	817.3
J. Tsui	Aluminum	AA5059	695.4	816.5
J. Tsui	Aluminum	AA5059	726.7	817.3

Table A.7: Maximum temperature from the literature and estimation of maximum temperature for each experiment part 7.

Author	Material	Especification	T_s [°K]	$\widehat{T_s}$[°K]
J. Tsui	Aluminum	AA5059	730.7	830.0
J. Tsui	Aluminum	AA5059	712.1	817.3
J. Tsui	Aluminum	AA5059	747.6	817.3

Annex B. Summary of torque data compiled from literature

Table B.1: Torque values from the literature and estimation of torque for each experiment part 1.

Author	Material	Especification	M[Nm]	$\widehat{M}$[Nm]
H. Schmidt	Aluminum	AA2024	40.0	37.7
K. J. Colligan	Aluminum	AA5083	295.0	471.1
K. J. Colligan	Aluminum	AA5083	326.0	481.8
K. J. Colligan	Aluminum	AA5083	358.0	494.4
T. Long	Aluminum	AA5083	181.0	367.5
T. Long	Aluminum	AA5083	152.0	277.3
T. Long	Aluminum	AA5083	128.0	223.8
T. Long	Aluminum	AA5083	108.0	184.5
T. Long	Aluminum	AA5083	94.0	155.3
T. Long	Aluminum	AA5083	79.0	125.2
T. Long	Aluminum	AA5083	70.0	108.9
T. Long	Aluminum	AA5083	64.0	92.8
T. Long	Aluminum	AA5083	50.0	75.8
T. Long	Aluminum	AA5083	40.0	64.3
T. Long	Aluminum	AA5083	35.0	55.9
T.J. Lienert	Aluminum	AA5083	23.7	32.3
M. Z. H. Khandkar	Aluminum	AA6061	84.4	131.5
T.J. Lienert	Aluminum	AA6061	30.6	25.5
A.P. Reynolds	Aluminum	AA7050	73.5	141.8
A.P. Reynolds	Aluminum	AA7050	118.4	197.2
A.P. Reynolds	Aluminum	AA7050	171.6	147.4
A.P. Reynolds	Aluminum	AA7050	78.4	98.3
A.P. Reynolds	Aluminum	AA7050	69.3	84.5
A.P. Reynolds	Aluminum	AA7050	63.7	66.2
A.P. Reynolds	Aluminum	AA7050	26.5	28.8
A.P. Reynolds	Aluminum	AA7050	79.9	142.4
A.P. Reynolds	Aluminum	AA7050	65.8	106.7
A.P. Reynolds	Aluminum	AA7050	53.5	71.8
A.P. Reynolds	Aluminum	AA7050	41.8	48.6
A.P. Reynolds	Aluminum	AA7050	32.1	36.5
A.P. Reynolds	Aluminum	AA7050	106.1	296.3
A.P. Reynolds	Aluminum	AA7050	101.4	194.2
A.P. Reynolds	Aluminum	AA7050	85.6	140.0

Table B.2: Torque values from the literature and estimation of torque for each experiment part 2.

Author	Material	Especification	M[Nm]	$\widehat{M}$[Nm]
A.P. Reynolds	Aluminum	AA7050	73.8	97.9
A.P. Reynolds	Aluminum	AA7050	62.8	84.5
A.P. Reynolds	Aluminum	AA7050	54.8	64.7
T. Long	Aluminum	AA7050	305.0	701.2
T. Long	Aluminum	AA7050	275.0	495.0
T. Long	Aluminum	AA7050	205.0	382.5
T. Long	Aluminum	AA7050	155.0	290.2
T. Long	Aluminum	AA7050	130.0	233.7
T. Long	Aluminum	AA7050	90.0	195.7
T. Long	Aluminum	AA7050	75.0	168.3
T. Long	Aluminum	AA7050	70.0	145.1
T. Long	Aluminum	AA7050	60.0	105.2
T. Long	Aluminum	AA7050	55.0	80.9
T. Long	Aluminum	AA7050	50.0	76.5
P.A. Colgrove	Aluminum	AA7075	199.2	345.2
P.A. Colgrove	Aluminum	AA7075	221.3	362.4
P.A. Colgrove	Aluminum	AA7075	245.1	383.9
P.A. Colgrove	Aluminum	AA7075	224.4	401.4
P.A. Colgrove	Aluminum	AA7075	250.5	416.9
P.A. Colgrove	Aluminum	AA7075	270.6	435.1
P.A. Colgrove	Aluminum	AA7075	292.2	457.5
P.A. Colgrove	Aluminum	AA7075	342.2	488.9
P.A. Colgrove	Aluminum	AA7075	343.8	508.6
P.A. Colgrove	Aluminum	AA7075	356.3	531.3
P.A. Colgrove	Aluminum	AA7075	384.8	560.5
P.A. Colgrove	Aluminum	AA7075	311.5	552.8
P.A. Colgrove	Aluminum	AA7075	95.5	122.3
P.A. Colgrove	Aluminum	AA7075	119.4	135.8
P.A. Colgrove	Aluminum	AA7075	129.7	143.4
T.J. Lienert	Aluminum	AA7075	58.6	21.9
T.J. Lienert	Steel	SAE1018	55.0	102.3
R. Nandan	Steel	SAE1018	68.8	127.6
R. Nandan	Steel	SAE1018	70.9	127.7
R. Nandan	Steel	SAE1018	72.6	127.7
R. Nandan	Steel	SAE1018	75.5	127.8
R. Nandan	Steel	SAE1018	55.2	99.3
R. Nandan	Steel	SAE1018	58.0	99.3
R. Nandan	Steel	SAE1018	59.2	99.3

Table B.3: Torque values from the literature and estimation of torque for each experiment part 3.

Author	Material	Especification	M[Nm]	$\widehat{M}$[Nm]
R. Nandan	Steel	SAE1018	61.1	99.4
R. Nandan	Steel	SAE1018	45.6	81.2
R. Nandan	Steel	SAE1018	48.4	81.2
R. Nandan	Steel	SAE1018	49.8	81.3
R. Nandan	Steel	SAE1018	51.0	81.3
R. Nandan	Steel	SAE1018	38.9	68.7
R. Nandan	Steel	SAE1018	41.3	68.7
R. Nandan	Steel	SAE1018	42.8	68.8
R. Nandan	Steel	SAE1018	43.7	68.8
R.Jain	Aluminum	AA2024	16.0	67.5
R.Jain	Aluminum	AA2024	12.0	50.6
R.Jain	Aluminum	AA2024	12.0	40.5
B. Yang	Aluminum	AA2024	95.4	114.1
B. Yang	Aluminum	AA2024	76.8	69.6
B. Yang	Aluminum	AA2024	87.4	71.0
B. Yang	Aluminum	AA2524	124.2	214.8
B. Yang	Aluminum	AA2524	65.9	86.7
B. Yang	Aluminum	AA2524	46.1	55.1
F.F. Wang	Aluminum	AA2198	13.3	30.6
F.F. Wang	Aluminum	AA2198	10.8	20.4
F.F. Wang	Aluminum	AA2198	9.0	15.3
F.F. Wang	Aluminum	AA2198	8.4	12.2
J. Tsui	Aluminum	AA5059	6.7	8.8
J. Tsui	Aluminum	AA5059	6.0	19.5
J. Tsui	Aluminum	AA5059	10.0	28.9
J. Tsui	Aluminum	AA5059	10.3	19.5
J. Tsui	Aluminum	AA5059	8.0	19.5
J. Tsui	Aluminum	AA5059	3.2	8.8
J. Tsui	Aluminum	AA5059	5.7	19.5
J. Tsui	Aluminum	AA5059	12.4	28.9
J. Tsui	Aluminum	AA5059	6.7	19.5
J. Tsui	Aluminum	AA5059	7.4	19.5386436